Cell

Coupled scRNA-Seq and Intracellular Protein Activity Reveal an Immunosuppressive Role of TREM2 in Cancer

Graphical Abstract

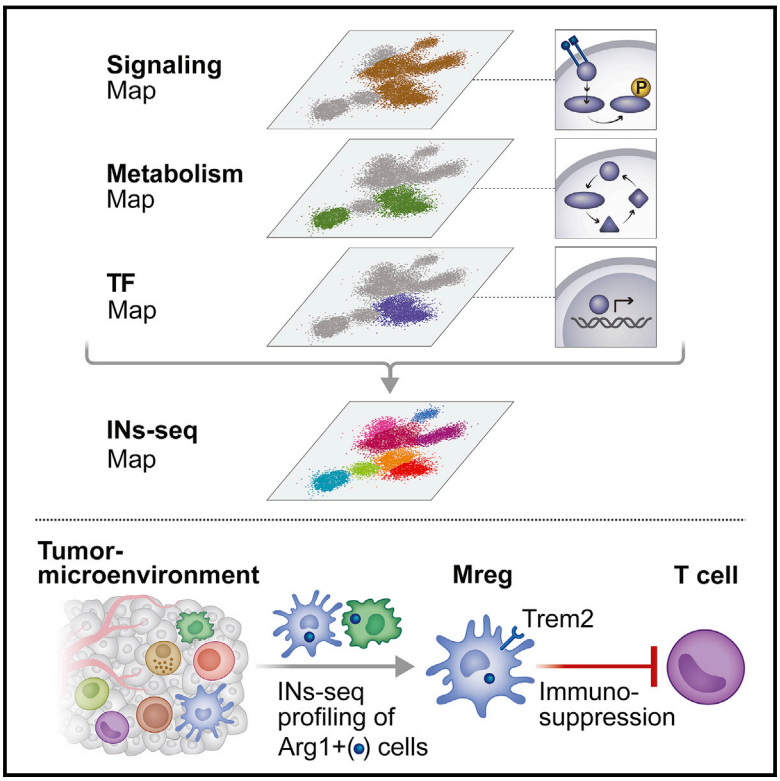

Highlights

- INs-seq: a new technology for recording scRNA-seq and intracellular protein activity
- INs-seq defines new immune subsets by TF combinations and metabolic activity
- Mapping Arg1^{+} cells within tumors reveals novel Trem2^{+} suppressive myeloid cells
- Genetic ablation of Trem2 decreases Mreg, exhausted CD8^{+} T cells and tumor growth

Authors

Yonatan Katzenelenbogen, Fadi Sheban, Adam Yalin, ..., Tomer-Meir Salame, Assaf Weiner, Ido Amit

Correspondence

assaf.weiner@weizmann.ac.il (A.W.), ido.amit@weizmann.ac.il (I.A.)

In Brief

INs-seq, an integrated technology for scRNA-seq and intracellular protein activity uncovers a novel Arg1+ Trem2+ regulatory myeloid cells (Mreg), genetic ablation of Trem2 inhibits the accumulation of intra-tumoral Mreg, leading to immune reactivation and reduced tumor growth.

Katzenelenbogen et al., 2020, Cell *182*, 872–885
August 20, 2020
https://doi.org/10.1016/j.cell.2020.06.032

CellPress

CellPress

Cell

Article

Coupled scRNA-Seq and Intracellular Protein Activity Reveal an Immunosuppressive Role of TREM2 in Cancer

Yonatan Katzenelenbogen,[1,3] Fadi Sheban,[1,3] Adam Yalin,[1,3] Ido Yofe,[1] Dmitry Svetlichnyy,[1] Diego Adhemar Jaitin,[1] Chamutal Bornstein,[1] Adi Moshe,[1] Hadas Keren-Shaul,[1] Merav Cohen,[1] Shuang-Yin Wang,[1] Baoguo Li,[1] Eyal David,[1] Tomer-Meir Salame,[2] Assaf Weiner,[1,4,*] and Ido Amit[1,4,5,*]

[1]Department of Immunology, Weizmann Institute, Rehovot 76100, Israel

[2]Flow Cytometry Unit, Life Sciences Core Facilities, Weizmann Institute of Science, Rehovot 76100, Israel

[3]These authors contributed equally

[4]Senior author

[5]Lead Contact

*Correspondence: assaf.weiner@weizmann.ac.il (A.W.), ido.amit@weizmann.ac.il (I.A.)

https://doi.org/10.1016/j.cell.2020.06.032

SUMMARY

Cell function and activity are regulated through integration of signaling, epigenetic, transcriptional, and metabolic pathways. Here, we introduce INs-seq, an integrated technology for massively parallel recording of single-cell RNA sequencing (scRNA-seq) and intracellular protein activity. We demonstrate the broad utility of INs-seq for discovering new immune subsets by profiling different intracellular signatures of immune signaling, transcription factor combinations, and metabolic activity. Comprehensive mapping of Arginase 1-expressing cells within tumor models, a metabolic immune signature of suppressive activity, discovers novel Arg1^{+} Trem2^{+} regulatory myeloid (Mreg) cells and identifies markers, metabolic activity, and pathways associated with these cells. Genetic ablation of Trem2 in mice inhibits accumulation of intra-tumoral Mreg cells, leading to a marked decrease in dysfunctional CD8^{+} T cells and reduced tumor growth. This study establishes INs-seq as a broadly applicable technology for elucidating integrated transcriptional and intracellular maps and identifies the molecular signature of myeloid suppressive cells in tumors.

INTRODUCTION

Cell fate and function are determined by integration of the cell's molecular composition with its metabolic and signaling activity. Recent advances in single-cell genomic technologies have provided an unprecedented amount of data on the RNA, protein, and chromatin states of cells within tissues (Griffiths et al., 2018; Kanton et al., 2019; Zeisel et al., 2018). These advances have dramatically improved the way we understand the cellular and molecular makeup of tissues and how they are perturbed during pathology (Linde et al., 2018; Segerstolpe et al., 2016). Despite these important developments, we still lack technologies that effectively link cellular transcriptional states with intracellular, post-translational states, such as those linked to signaling pathway activation and metabolic activity. Recent breakthroughs have linked single-cell transcriptomics data with quantitative protein measurements using index sorting (MARS-seq, GateID; Baron et al., 2019; Jaitin et al., 2014; Paul et al., 2015) or barcoded antibodies (CITE-seq, REAP-seq; Peterson et al., 2017; Stoeckius et al., 2017), but all are limited to cell surface proteins, whereas most of the signal transduction, metabolic, and transcriptional pathways are intracellular. Transcription factor (TF) combinations define the cell developmental trajectory together with its potential to respond to extracellular signals and have been shown to represent homogeneous cell subsets more precisely than surface markers (Schaum et al., 2018). In line with this, engineered TF reporter models play a critical role in defining new immune subsets (Josefowicz and Rudensky, 2009; Murphy et al., 2016) but are difficult to scale or use in a human context because they are dependent on engineered animal models.

To record the activity of intracellular proteins, cell fixation and permeabilization are required. Current cell fixation and permeabilization methods are destructive to mRNA integrity, limiting our ability to measure the intracellular protein landscape along with RNA sequencing (RNA-seq) in single cells. So far, efforts to combine single-cell RNA-seq (scRNA-seq) with fixation, permeabilization, and intracellular readouts have been difficult to scale and are limited to simple tissue culture models (Alles et al., 2017; Gerlach et al., 2019; Yamada et al., 2010). Technologies that enable transcriptional and intracellular protein profiling can potentially be a cornerstone for a better understanding of the interplay between epigenetic, transcriptional, signaling, and metabolic circuits that govern cellular function. Such

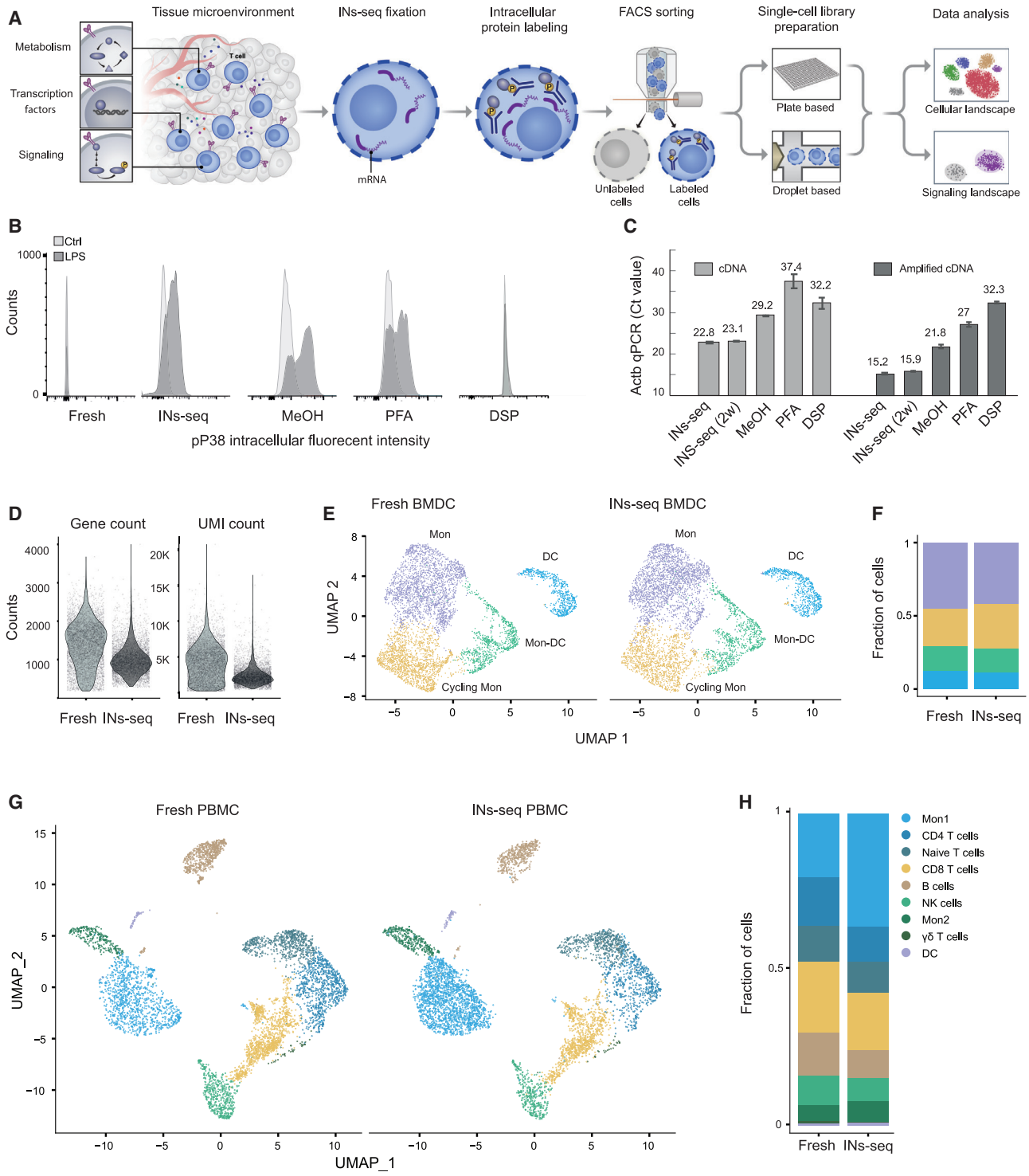

Figure 1. INs-Seq: An Integrated Technology for scRNA-Seq and Intracellular Protein Measurements

(A) Schematic of the INs-seq experimental approach.

(B) Flow cytometry histogram of pp38 fluorescence intensity of fresh cells, INS-seq, PFA-fixed, methanol-fixed and DSP-fixed cells (dark gray for LPS-treated cells and light gray for control cells).

(C) qPCR Cycle threshold (Ct) values of mouse Actb cDNA after reverse transcription (cDNA-Ct) and reverse transcription followed by PCR amplification (amplified cDNA-Ct) for INs-seq BMDC and other fixation protocols. Error bars indicate mean ± SEM.

(D) Violin plots of gene count and unique molecular identifier (UMI) count of 5,476 fresh and 5,454 INs-seq BMDC.

(legend continued on next page)

technologies can be utilized to characterize complex cellular responses, such as the immune response to pathogens, cancer, and other pathologies.

Immune cells sense and respond to a large array of environmental signals, such as pathogen-associated molecular patterns. These signals are recognized by specialized receptors (e.g., Toll-like receptors [TLRs]) and processed by intracellular signaling cascades to ultimately activate a variety of transcriptional and metabolic pathways that govern the immune response (Kumar et al., 2011). Characterization of these intracellular signaling pathways is mostly studied using established cell surface markers. This methodology potentially biases our knowledge of signaling and metabolic activities associated with diverse immune functions.

One example of such elusive and poorly characterized immune function is myeloid-derived suppressor cells (MDSCs), known to promote a suppressive environment for effector T cells within the tumor microenvironment (TME) and support tumor growth and immune dysfunction (Gabrilovich, 2017; Gabrilovich and Nagaraj, 2009). Despite MDSCs' critical effect on treatment outcome in a broad spectrum of human disease and cancer types, their precise functional roles and molecular identity have been elusive and ill defined. MDSCs do not conform to conventional surface marker-based classification schemes and are classified using broad myeloid surface markers, various cellular assays, and metabolic properties, including expression of an immunosuppressive metabolic pathway expressing Arginase 1 (Arg1) (Arlauckas et al., 2018; Veglia et al., 2018). A thorough molecular understanding of this important and heterogeneous group of myeloid cells, based on their suppressive metabolic potential, may lead to identification of their molecular markers, pathways, and activity, ultimately leading to more effective biomarkers and targeted immunotherapy.

Together, these challenges highlight the need for new single-cell technologies capturing transcriptional and intracellular protein activity. Here we present intracellular staining and sequencing (INs-seq) integrated technology that combines the resolution of massively parallel scRNA-seq with intracellular protein measurements. We demonstrate the potential of INs-seq for profiling intracellular and post-translationally modified proteins (PTM), signaling pathways, TFs, and metabolism-related proteins combined with scRNA-seq. Using INs-seq, we define the response of bone marrow myeloid culture to the TLR4 agonist lipopolysaccharide (LPS). Single-cell profiling of phospho-p38 mitogen-activated protein kinase (pp38 MAPK (pT180/pY182))-positive and -negative cell populations identified that dendritic cells are not responsive to an LPS signal, in contrast to monocytes. We further demonstrate the specificity of our technology by profiling regulatory T (Treg) cells, which have no specific surface marker, using intracellular immunostaining of the Treg cell-specific TF FOXP3 in human peripheral blood mononuclear cells (PBMC) and mice and benchmark these results to Foxp3-RFP transgenic mice. INs-seq profiling of the TFs TCF7, ID2, and TCF7 and ID2 double-positive populations shows the potential of the technology to define new T cell subsets. Finally, we focus on characterizing MDSCs based on their metabolic features to reveal their cellular and molecular profile in the TME and identify markers and pathways specific for MDSCs. Our data revealed a new Trem2^{+} regulatory monocyte population, regulatory myeloid (Mreg) cells, as major myeloid suppressive cells in a mouse fibrosarcoma syngeneic tumor model. Genetic ablation of Trem2 in these mice inhibits accumulation of Mreg cells, leading to a significant decrease in dysfunctional CD8^{+} T cells and reduced tumor growth. This study establishes INs-seq as a broadly applicable technology for elucidating integrated transcriptional and signaling maps and identifies the molecular signature of myeloid suppressive cells.

RESULTS

INs-Seq: An Integrated Technology for scRNA-Seq and Intracellular Protein Measurements

To integrate the intracellular signaling state and the cellular transcriptional profile, we developed INs-seq, an integrative technology for intracellular protein immunodetection followed by scRNA-seq (Figure 1A). In this protocol, cells are fixed and permeabilized using a fixative based on methanol (MeOH) and ammonium sulfate solutions that precipitates proteins, inhibits enzymatic activity, and enables RNA preservation and immuno-intracellular staining (STAR Methods). The permeabilized cells can then be labeled intracellularly with fluorophore-conjugated antibodies and sorted by fluorescence-activated cell sorting (FACS) according to their intracellular fluorescent signal intensity, followed by scRNA-seq using plate-based or microfluidics-based approaches (STAR Methods).

To evaluate INs-seq efficiency in preserving mRNA and allowing simultaneous intracellular labeling, we compared INs-seq fixation with three commonly used fixation methods: PFA (paraformaldehyde), methanol, and DSP (dithiobis(succinimidyl propionate)). We differentiated mouse bone marrow-derived cells in the presence of GM-CSF (BMDC culture) and stimulated the culture with LPS for 20 min. We then processed the cultured cells using INs-seq fixation or the three other fixation methods. Cells were stained for the extracellular markers CD11c and Ly6G and sorted for CD11c^{+}, Ly6G^{-} (BMDC) and the intracellular active form of the p38 MAPK, phospho-p38 (pT180/pY182). Cells processed by PFA, MeOH, and INs-seq (but not DSP) showed a clear fluorescent pp38 signal (Figure 1B). Further, INs-seq fixation was compatible with a wide range of commonly used FACS fluorophores (Figure S1A; see STAR Methods for recommended INs-seq fluorophores). To quantify preservation of mRNA by the different fixation protocols, we extracted mRNA from 5,000 sorted BMDC, generated cDNA, and amplified cDNA from the isolated cells. Quantitative PCR (qPCR) measurement of the housekeeping gene β-actin (*Actb*) showed marked

(E and F) Uniform Manifold Approximation and Projection (UMAP) of scRNA-seq data from fresh and INs-seq CD11c^{+}Ly6G^{-} BMDC (E). The color code for cell type assignment is indicated in the plot, with (F) the fraction of the different cell types in each sample.
(G and H) UMAP of scRNA-seq data from 9,053 fresh and 5,620 INs-seq fixed human blood PBMC (CD45^{+} immune cells) (G). The color code for cell type assignment is indicated in the plot, with (H) the fraction of the different cell types in each sample.
See also Figures S1 and S2.

differences between the protocols (Figure 1C). INs-seq preserved 84-fold more *Actb* mRNA molecules compared with the second-best fixation method (MeOH fixation) and more than 600-folds more over PFA and DSP. Similar results were obtained from mouse and human primary cell types (Figure S1B). Additionally, INs-seq enabled almost complete preservation of mRNA of fixed cells stored at −20°C for up to at least 2 weeks (Figure 1C). Importantly, INs-seq-fixed samples demonstrated a minor reduction in mRNA detection compared with fresh non-fixed samples (Figure S1C).

To further examine the quality of INs-seq fixation, we constructed scRNA-seq libraries using the droplet-based chromium platform from fresh and INs-seq-fixed BMDC. We used the Seurat integration workflow to integrate INs-seq and fresh samples and clustered them together (Stuart et al., 2019). INs-seq-processed cells displayed a 50%–60% reduction in the number of unique molecular identifiers (UMIs) per cell compared with fresh cells (Figure 1D). However, this reduction in UMI count was uniform and not biased toward any specific cell type. Therefore, despite this mRNA loss, INs-seq preserves the same cell population distribution observed in fresh, non-fixed cells (Figures 1E and 1F). Compared with scRNA-seq of fresh cells, INs-seq preferably samples long genes (>10 kb), including non-coding RNA, over short genes (<1,000 bp), suggesting that some RNA fragmentation still occurs during sample processing (Figures S1D and S1E). However, clustering and projection of the fresh and INs-seq data on the same manifold identify the same differential genes and dynamic ranges between the cell populations (Figures 1F and S1F; Table S1). To evaluate the robustness and clinical potential of INs-seq, we fixed human PBMC samples (STAR Methods). Comparison of fresh and INs-seq-fixed CD45$^+$ immune blood cells from three individuals shows an overall high similarity in cell population distribution, except a small enrichment of one monocyte population in the INs-seq samples (Figures 1G, 1H, and S2A–S2C; Table S2). Together, these results demonstrate the efficiency of INs-seq in labeling intracellular proteins while preserving the mRNA content in single cells.

INs-Seq Identifies Dendritic Cells as a pp38$^-$ Fraction in BMDC Culture

The myeloid compartment is composed of diverse cell types and states that respond differently to environmental signals (Glass and Natoli, 2016; Jaitin et al., 2016). To better understand the complexity of the myeloid response to pathogen signals, we stimulated the bone marrow culture with LPS and performed INs-seq fixation and intracellular staining with fluorescent pp38, a downstream component of the TLR4 signaling cascade (Amit et al., 2009; Kumar et al., 2011). The BMDC cultures were then sorted by FACS according to the intensity of their pp38 signal and processed using the chromium platform (Figures 2A and S3A). We used the Seurat integration and clustering workflow and identified 4 clusters of cells from the BMDC scRNA-seq data, including monocytes, cycling monocytes, dendritic cells (DCs) and a monocyte-DC population (Figure 2B). By quantification of pp38 enrichment score in each cluster, based on its fraction in the pp38$^+$ over pp38$^-$ populations, we identified a significant depletion of the DC population. The DC (e.g., expressing *Ccr7*, *Ccl22*, and the major histocompatibility complex [MHC] class II pathway) population was dramatically diminished in the pp38$^+$ fraction (Figures 2C, 2D, and S3B).

LPS is mainly sensed through the TLR4 pathway and its co-receptor CD14, which regulates TLR4 endocytosis (Zanoni et al., 2011). Comparison of the expression of TLR4 and CD14 in the BMDC populations showed diminished gene expression of TLR4, CD14, and the major TLR4 signaling adaptor MyD88 in DCs compared with the other cell populations in the culture (Figure 2E). Correspondingly, FACS analysis of monocytes (CD14^{high} CD11c$^+$) cells showed a high pp38 signal compared with the DC (CD14^{low} CD11c$^+$) population (Figure S3C). In line with these findings, DC (MHC class II^{high} CD11c$^+$) showed a decreased pp38 signal compared with monocytes (MHC class II^{mid} Cd11c$^+$; Figure 2F; Helft et al., 2015). Moreover, LPS stimulation of BMDC resulted in a minor inflammatory response in the DC population compared with a massive response of the monocyte populations (Figure 2G). In summary, we demonstrate INs-seq to be a robust technology for single-cell characterization of transcriptional and signaling activity and show that signaling downstream of LPS stimulation is blunted in DCs compared with monocytes, including the pp38 MAPK and downstream inflammatory cytokines.

Comprehensive Cell Type Characterization by TF Targeting

The complex gene expression programs that underlie development, differentiation, and environmental responses are determined by binding of sequence-specific TFs. TF combinations may faithfully define the cell's developmental trajectory together with its prospect to respond to extracellular signals and can potentially be applied for precise cell characterization of diverse immune subsets. So far, genetic engineering of TF reporters, with all of its limitations, is the major approach for such efforts and is an instrumental tool for discovery of novel immune populations. The TF factor Foxp3, a master regulator of Treg cell development and function, is the only discriminative marker to purify Treg cells from other T cells (Kim and Rudensky, 2006). Currently, cell surface markers used for purification and characterization of Treg cells in different tissues and pathologies are limited (Chen and Oppenheim, 2011). To assess INs-seq efficiency for *in vivo* mapping of Treg cells, we used a Foxp3-RFP transgenic mouse expressing a fluorescent Foxp3 reporter (Tg(Foxp3-RFP,-cre); STAR Methods), where the Foxp3 promoter drives the expression of RFP and Cre recombinase. We enriched for Treg cells from Foxp3-RFP cervical lymph nodes (cLNs) by sorting TCRb$^+$ RFP$^+$ cells or applying the INs-seq protocol and sorting antibody-stained TCRb$^+$ Foxp3$^+$ cells (Figures 3A and S4A). scRNA-seq libraries were constructed from unfixed Foxp3-RFP$^+$ and fixed Foxp3$^+$ cells (STAR Methods). Analysis of the scRNA-seq data of 5,483 cells created a map of the cell types profiled in Foxp3$^+$ fixed and RFP$^+$ unfixed cLN samples and identified similar Treg cell enrichments using genetic and antibody-based Foxp3$^+$ strategies (Figures 3B, S4B, and S4C; 80% and 60%, respectively). Similarly, isolated Treg cells from both strategies demonstrated expression of the same Treg cell gene modules and markers (Figure S4D).

Treg cells are key mediators of immunosuppression within the TME (Magnuson et al., 2018; Togashi et al., 2019). To

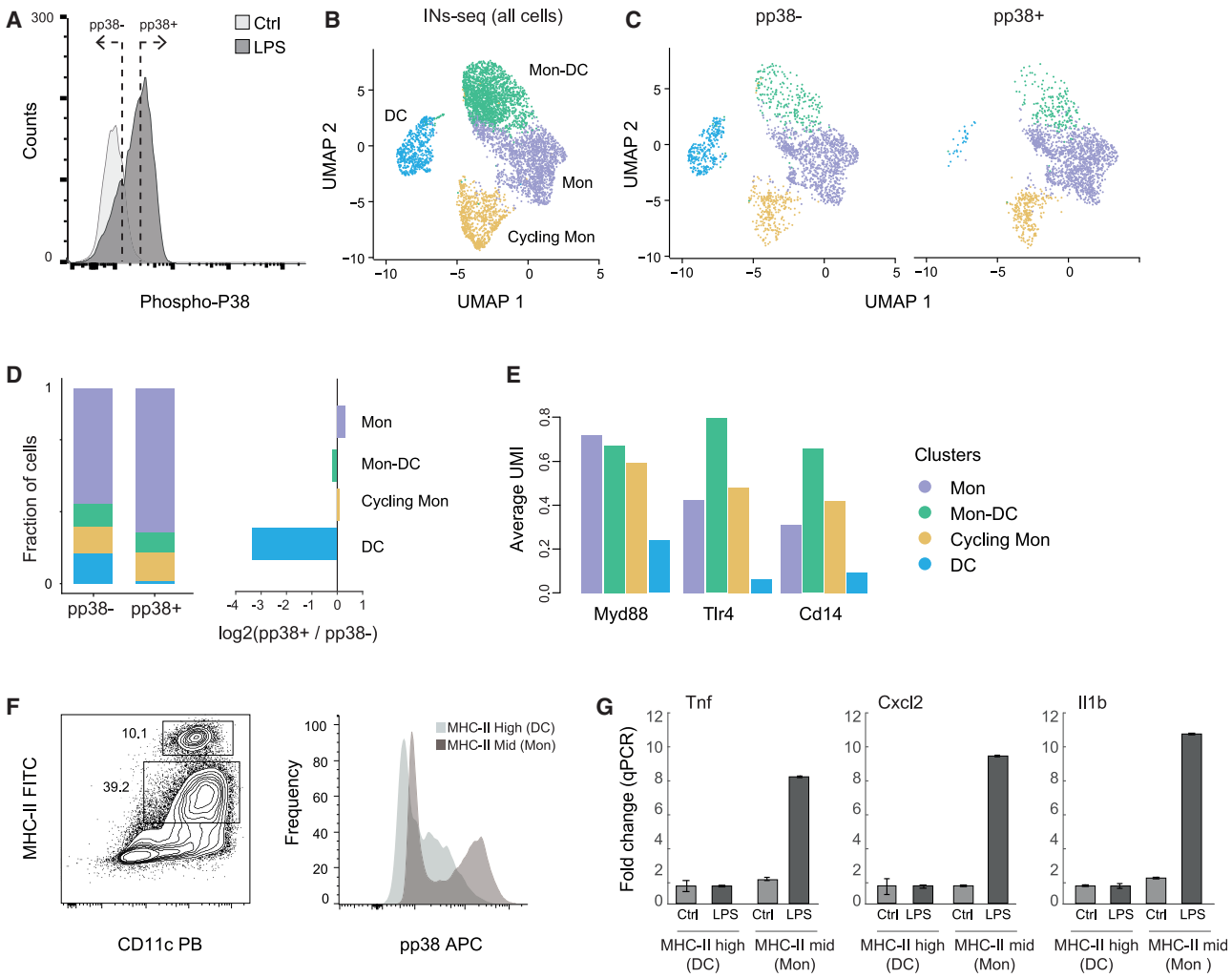

Figure 2. INs-Seq Detects pp38 MAPK Activity in BMDC Culture following LPS Stimulation

(A) Flow cytometry histogram of the pp38 signal in LPS-treated and control BMDC; the gating strategy for pp38^{+} and pp38^{-} cells is shown.

(B) UMAP representation of QC-positive scRNA-seq data of 4,169 INs-seq pp38^{+} and pp38^{-} cells. Different colors represent different cell population, as indicated in the plot.

(C) UMAP split to 2,091 INs-seq pp38^{+} cells and 2,078 pp38^{-} BMDC.

(D) Relative fraction of the 4 clusters in pp38^{+} and pp38^{-} samples (left). Shown is a log2 plot of pp38^{+} over pp38^{-} for each cell population (right)

(E) Average UMI count of Myd88, Tlr4, and CD14 in each cell population.

(F) Flow cytometry histogram plots of the pp38 fluorescence signal of CD11c^{+}MHCII^{high} and CD11c^{+}MHCII^{mid} BMDC.

(G) qPCR analysis (ΔΔCt) of *Tnf*, *Cxcl2*, and *Il-1b* four hours after LPS stimulation of CD11c^{+}MHCII^{high} and CD11c^{+}MHCII^{mid} BMDC compared with control BMDC. Error bars indicate mean ± SEM.

See also Figure S3.

compare the molecular profiles of cLN and tumor Treg cells, we isolated tumor-infiltrating lymphocytes (TILs), and applied INs-seq to profile the TME CD45^{+} TCRb^{+} Foxp3^{+} and CD45^{+} TCRb^{+} Foxp3^{-} cell populations. Analysis identified that the Foxp3^{+} population contained Treg cells and related transcriptomics signatures, comprising high levels of expression of *Foxp3*, *Ctla4*, *Il2ra*, and different members of the tumor necrosis factor (TNF) receptor family (e.g., *Tnfrsf4* and *Tnfrsf18*) (Figure S5A). In line with previous studies, Treg cells isolated from cLNs expressed a gene module related to naive and circulating T cells, such as *Ccr7*, *Tcf7*, and *Lef1* (Ricardo Miragaia et al., 2019; Tong et al., 2019), whereas Treg cells isolated from the TME exhibited an active Treg cell-suppressive phenotype, expressing high levels of *Gzmb*, *Ccr2*, and the TNF receptor family members 18 and 9 (Azizi et al., 2018; Cao et al., 2007; Figure 3C). In summary, by targeting the Treg cell-specific TF Foxp3 from the mouse circulation (lymph nodes) and TME, we demonstrate application of the INs-seq technology to combine TF labeling with scRNA-seq.

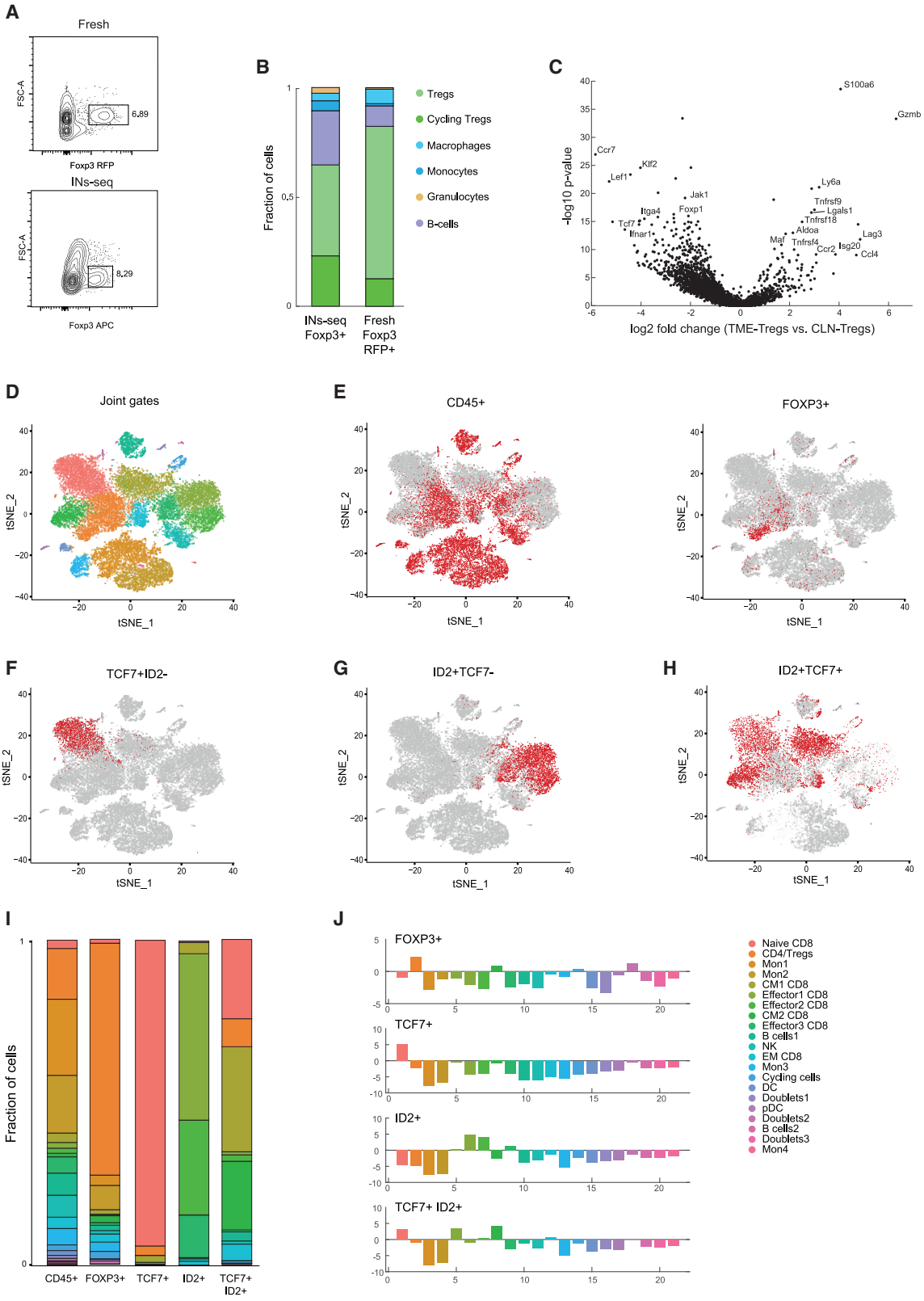

(legend on next page)

T Cell INs-Seq TF Map Defines the Signature of Memory T Cells

We next aimed to define the molecular identity of diverse T cell states in human PBMC. For this we applied INs-seq and targeted a combination of key TFs involved in T cell biology: FOXP3, the master regulator of the Treg cell phenotype, and two major CD8 T cell TFs, T cell factor 7 (TCF7) and inhibitor of DNA binding 2 (ID2). We applied the INs-seq protocol on PBMC and gated for $CD3^+FOXP3^+$; $CD8^+$,$TCF7^+$; $ID2^+$ single-positive (SP); or $TCF7^+ID2^+$ double-positive (DP) T cells. We then sequenced these populations, resulting in 14,245 cells (Figures S5B and S5C; Table S3). The $CD3^+FOXP3^+$ sample was then compared with the whole PBMC fraction from the same donor and showed enrichment of human CD4 Treg cells, expressing the canonical Treg cell markers *FOXP3*, *TNFRSF4*, *IL2RA*, *IKZF2,* and *TIGIT* (Figures 3D, 3E, and S5D). Although FOXP3 is an example of an extensively studied cell-type-specific TF in humans and mouse models, the functional roles of TCF7 and ID2 T cell subsets are only partially characterized. TCF7 is a critical regulator of T cell development and self-renewal potential (Kratchmarov et al., 2018; Shah and Zúñiga-Pflücker, 2014). Upon antigen encounter and effector differentiation, CD8 T cells require ID2 for survival and proliferation (Cannarile et al., 2006; Yang et al., 2011). TCF7 and ID2 have been shown to be expressed in memory CD8 T cells and to play a key role in CD8 T cells during viral infection and tumor progression (Held et al., 2019; Im et al., 2016; Masson et al., 2013); however, the exact interplay of these two essential elements in dictating CD8 T cells states is still unclear. Notably, CD8 T cells lacking both of these TFs (double-negative) were not observed, exemplifying their importance in controlling CD8 T cell states (Figure S5C).

In line with previous studies (Willinger et al., 2006; Zhou et al., 2010) the $TCF7^+$ gate showed expression of gene modules associated with a naive phenotype, such as *CCR7*, *SELL*, and *LEF1* (Figure S5E). This population occupies 94% of the $TCF7^+$ gate with a 36-fold enrichment compared with the fraction of this population in the $CD45^+$ immune gate (Figures 3F, 3I, and 3J). In contrast, the $ID2^+$ gate was characterized with CD8 T cell effector functions, expressing many of the genes associated with the cytotoxic machinery (*GNLY*, *GZMA/B*, and *PRF1*) alongside other markers of cytotoxic T cells, such as *NKG7*, *FGFBP2*, and *CX3CR1* (Figure S5E). The effector cells occupied 93% of the $ID2^+$ gate with 11-fold enrichment compared with their fraction in the $CD45^+$ immune population (Figures 3G, 3I, and 3J). The $TCF7^+$ $ID2^+$ DP gate defined less characterized T cell subsets and was specifically enriched for two cell states of central memory (CM) and one state of effector memory (EM) T cells (Figure 3H). The two CM phenotypes share expression of *KLRG1* and *ITGB1* as well as naive markers such as *CCR7* and *SELL*. The CM phenotypes segregated based on expression of *CXCR3*, *CCL5*, and *GZMK* in CM1 and *TNFRSF4* in CM2 (Figure S5E). EM cells express low levels of the naive markers and are characterized by expression of *GZMK*, *KLRG1*, *KLRB1*, and *PRF1*. Altogether, we demonstrate INs-seq to be a powerful tool for studying the interplay between different TFs in controlling cellular state in humans and mice at the single-cell level.

Trem2 Defines Two Populations of Tumor-Infiltrating Myeloid Suppressive Cells

Myeloid cells play a key role in controlling activation and inhibition of adaptive anti-tumor responses. However, to date, there are no clear cell surface molecules other than broad lineage markers (CD11b and Gr-1) to define myeloid suppressive cells, limiting molecular and functional characterization of this important lineage. The Arg1 enzyme, which metabolizes arginine to urea and ornithine, supports many physiological processes, such as liver function and collagen production (Caldwell et al., 2018). Within the immune compartment, suppressive myeloid populations activate the Arg1 pathway, depriving the microenvironment of arginine, an essential amino acid for T cell activity (Bronte et al., 2003). Arg1, alongside other metabolic proteins, is a hallmark of tumor-associated myeloid suppressor cells that accumulate under pathological conditions (Gabrilovich, 2017; Kumar et al., 2016). To deeply characterize myeloid suppressor cells within the TME, we applied INs-seq to isolate and profile Arg1-expressing cells from a mouse tumor model and define their cellular and molecular pathways (Figure 4A).

We fixed and sorted by FACS $CD45^+$ $CD11b^+$ $Arg1^+$ and $CD45^+$ $CD11b^+$ $Arg1^-$ cell populations from the TME of MCA205 tumor-bearing mice (Figure S6A). Of 8,280 QC-positive cells, we removed the lymphoid, granulocyte, and DC populations from the myeloid Arg1 map for separate analysis. 7,648 cells were defined as monocytes and macrophages based on marker genes expression (STAR Methods). Metacell analysis identified 77 metacells comprising 6 distinct populations (Figures 4B and 4C; Table S4). For each metacell, we computed an Arg1 enrichment score based on its fraction in the $Arg1^+$ over $Arg1^-$ populations (Figures 4B). We found high correlation between the Arg1 enrichment score and its transcription levels (Figures S6B–S6D). The myeloid compartment in the TME was characterized by two major $Arg1^+$ populations: tumor-associated macrophages (TAMs), distinguished by expression of *C1qa*, *Spp1*, *Cx3Cr1*, and *Apoe*, and an Mreg cell population expressing *Gpnmb*, *Il7r*, *Hilpda*, *Vegfa*, *Hmox1*, and *Clec4d*,

Figure 3. Characterization of T Cell Subtypes by INs-Seq TF Maps

(A) FACS plots showing the gating strategy for fresh $TCRb^+Foxp3\text{-}RFP^+$ and INs-seq $TCRb^+APC\text{-}Foxp3^+$ populations isolated from (Tg(Foxp3-RFP,-cre) cLNs.

(B) Percentage of the different clusters in fresh $TCRb^+Foxp3\text{-}RFP^+$ compared with INs-seq $TCRb^+APC\text{-}Foxp3^+$ populations.

(C) Volcano plot showing the gene expression fold change of TME Treg cells versus cLN Treg cells (x axis) and their Mann-Whitney p values (y axis).

(D) t-Distributed Stochastic Neighbor Embedding (tSNE) of scRNA-seq data from 29,376 INs-seq-fixed human blood PBMC; all gates combined ($CD45^+$, $CD3^+FOXP3^+$, $CD8^+TCF7^+ID2^-$, $CD8^+ID2^+TCF7^-$, $CD8^+ID2^+TCF7^+$). The color code for cell cluster assignment is as indicated in (J).

(E) Projection of cells from the different gates onto the tSNE plot: 15,131 $CD45^+$ cells (left panel) and 1,231 $Foxp3^+$ cells (right panel).

(F–H) tSNE plot of (F) 2,195 $CD8^+TCF7^+ID2^-$ cells, (G) 4,257 $CD8^+ID2^+TCF7^-$ cells, and (H) 6,562 $ID2^+TCF7^+$ cells.

(I) Cell type distribution of the different PBMC gates.

(J) Enrichment of the different cell types for each gate over the $CD45^+$ gate (log2 scale). The color code for cell cluster assignment is as in (D).

See also Figures S4 and S5.

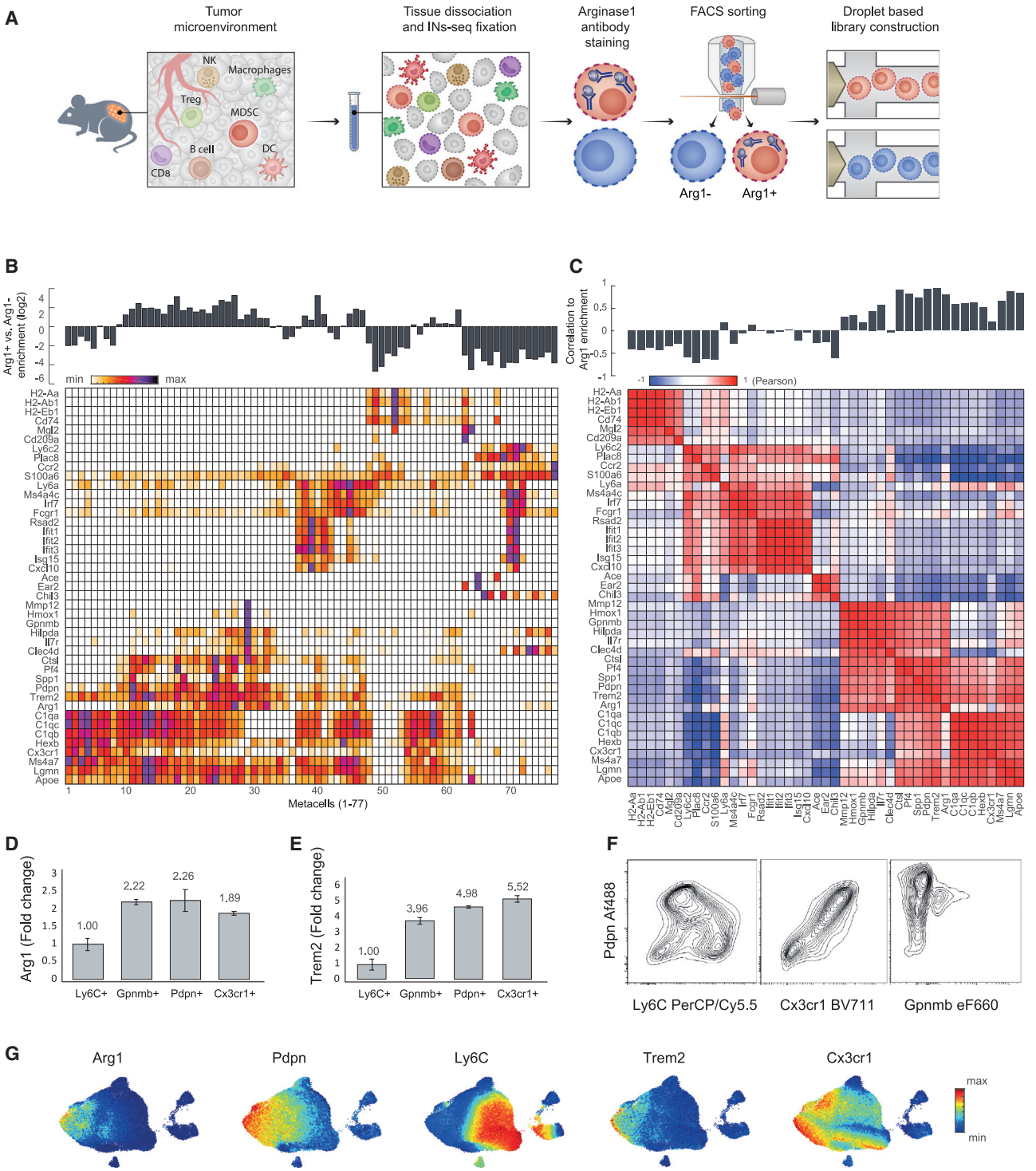

Figure 4. Trem2 Defines Two Populations of Tumor-Infiltrating Myeloid Suppressive Cells

(A) Schematic of the experimental design.

(B) Gene expression heatmap of 42 genes from 7,648 cells clustered into 77 metacells of Arg1^{+} and Arg1^{-} cells. The top bar plot shows the Arg1 enrichment score (fraction in the Arg1^{+} over Arg1^{-} samples).

(C) Gene-gene Pearson correlation heatmap of 42 markers genes within the Arg1^{+} and Arg1^{-} metacells. The top bar plot shows the Pearson correlation between gene expression and Arg1 enrichment score.

(D and E) qPCR analysis of *Arg1* (D) and *Trem2* (E) expression fold change in the different cell populations compared with Ly6C^{+}. Error bars indicate mean ± SEM.

(legend continued on next page)

among other differentially expressed genes (Figures 4B and 4C). The four Arg1$^-$ populations could be distinguished by expression of specific markers: *Plac8*, *Ly6c2*, *Ccr2*, MHC class II-related genes, and a signature associated with type I interferon signaling (Figures 4B and 4C). Analysis of the Arg1$^+$ and Arg1$^-$ metacells resulted in the *de novo* identification of a rich set of co-regulated gene modules (Figure 4C). This analysis further identified Podoplanin (*Pdpn*) and triggering receptor expressed on myeloid cells 2 (*Trem2*) as genes significantly correlated with Arg1 expression in the TAM and Mreg cell populations (Figures 4C and S6C–S6E).

Recent discoveries establish the TREM2 receptor as a major pathology-induced myeloid cell signaling hub that activates immune remodeling in response to tissue damage (Ulland and Colonna, 2018; Zheng et al., 2018). Trem2 has been shown to orchestrate immunosuppressive, phagocytosis, and survival functions in myeloid cells associated with neurodegenerative and metabolic pathologies (Deczkowska et al., 2020; Jaitin et al., 2019; Keren-Shaul et al., 2017). To validate our findings, we next used the surface markers identified in scRNA-seq to enrich for the myeloid suppressive cells expressing high Arg1 protein and then measured their *Arg1* and *Trem2* mRNA quantities using qPCR. We used antibodies targeting Pdpn, Cx3cr1, and Gpnmb because they defined distinct markers for the two major Arg1^{high} subpopulations, whereas Ly6C$^+$ cells were correlated with the Arg1^{low} subsets. Consistent with our data, qPCR analysis of Pdpn, Gpnmb, and Cx3cr1 populations detected higher expression levels of *Arg1* and *Trem2* transcripts compared with the Ly6C$^+$ population (Figures 4D and 4E).

To further validate our results, we analyzed CD45$^+$ CD11b$^+$ cells from MCA205 mouse tumors stained for the same cell surface markers depicting the different Arg1$^+$ and Arg1$^-$ intra-tumoral myeloid populations within the TME. We validated that Pdpn^{high} and Ly6C^{high} subsets were clearly detectable as separate populations by flow cytometry. Furthermore, the Pdpn^{high} myeloid population was strongly associated with Cx3cr1^{high} and Gpnmb^{high} markers (Figure 4F). To further devise a sorting strategy and characterize the Arg1$^+$ and Arg1$^-$ intra-tumoral myeloid populations, we used CyTOF mass cytometry to profile the intra-tumoral immune populations of MCA205. Analysis of a large set of proteins defined by our single-cell data revealed similar results as those observed in our FACS analysis (Figure 4G; STAR Methods). The CyTOF results further confirmed our transcriptional findings, defining two distinct myeloid populations marked by Pdpn and Ly6C. In line with the single-cell data, the Pdpn population overlapped with expression of Cx3cr1, Trem2, Arg1, and CD206 (Mrc1) (Figures 4G and S6F). In summary, INs-seq analysis of Arg1 expression defined the molecular characteristics of two distinct myeloid populations that share the expression of Arg1 and the Trem2 receptor: a TAM population and an Mreg cell population.

Trem2 Promotes T Cell Dysfunction and Tumor Immune Escape

To confirm our INs-seq tumor map and gain deeper molecular characterization of the tumor-associated myeloid populations, we sorted immune cells (CD45$^+$) from MCA205 tumors for MARS-seq analysis. We used the MetaCell algorithm to identify homogeneous groups of cells from scRNA-seq data, resulting in a map of 115 metacells (Figure S7A; Table S5). We removed the lymphoid, granulocyte, and DC populations and separately analyzed only myeloid populations (Figure 5A). Similar to our INs-seq tumor map, *Arg1* expression was highly correlated with *Trem2* and *Pdpn* expression, whereas *Ly6C*, *Ccr2*, and *Plac8* represented Arg1$^-$ myeloid populations (Figure 5B). Consistent with our analysis, the Arg1$^+$ Trem2$^+$ populations can be subdivided into two distinct programs: TAMs, characterized by mature macrophages markers such as *Cx3cr1*, *Apoe*, and *C1qa*, and Mreg cells, monocyte-like cells expressing *Gpnmb*, *Il7r*, and several hypoxia-related genes such as *Hilpda*, *Hmox1*, and *Vegfa* (Figures 5B–5D). We found multiple TFs that correlated with the myeloid suppressive programs, including known regulators and several TFs that have not been associated previously with myeloid suppressive cells (Figure 5E). We trained a lasso-regularized, cross-validated linear model (STAR Methods), predicting the different programs with high accuracy based on expression of TFs only (Figures 5E and S7C). We found *Maf*, *Cebpb*, *Atf3*, and *Hif1a* to be potential Mreg cell regulators and *Spi1* and *Hif1a* for TAMs. The monocytes cluster enriched with type I interferon signaling showed TF enrichment for *Stat1*, *Irf9*, and *Irf7*.

To better understand the regulatory mechanisms of Arg1$^+$ cells, we further analyzed the single-cell data, seeking potential regulators that may perturb accumulation of myeloid suppressive cells. Among them, we identified Trem2 as a promising target. Trem2 was highly correlated with Arg1$^+$ myeloid cells and has been shown to promote myeloid cell proliferation, survival, and immune suppression in various pathologies (Gervois and Lambrichts, 2019; Zhong et al., 2017). Trem2 has also been shown to be expressed in myeloid cells in human tumors, and its deficiency in a mouse tumor model abrogates tumor growth (Tang et al., 2019; Zhang et al., 2018). To define the function of Trem2 in the TME, we first screened for Trem2-expressing macrophage cell lines. We identified N9 cells as a relevant Trem2-expressing model and used CRISPR-Cas9 and *Trem2*-specific guide RNA to generate a Trem2-deficient N9 model (STAR Methods). To evaluate the functional effect of Trem2 on T cell activation, we co-cultured N9 or Trem2-deficient N9 cells in a 1:5 ratio with cell proliferation dye-labeled splenic naive CD8+ T cells activated with α-CD3 and α-CD28 (Figures S7D and S7E). CD8+ T cells co-cultured with N9 cells demonstrated significant suppression of CD8+ T cell proliferation comparable with, if not more suppressive, than addition of transforming growth factor β (TGF-β) to the medium. CD8+ T cells co-cultured with Trem2-deficient N9 cells showed a subtle effect on CD8+

(F) Representative flow cytometry plots of Pdpn versus Ly6C, Cx3cr1, and Gpnmb of cells isolated from the MCA205 CD45$^+$CD11b$^+$ population.
(G) UMAP projection of CyTOF data of MCA205 CD45$^+$ immune cells. Detected protein levels of Arg1, Pdpn, Ly6c, Trem2, and Cx3cr1 are shown by color gradient, as indicated in the plot.
See also Figure S6.

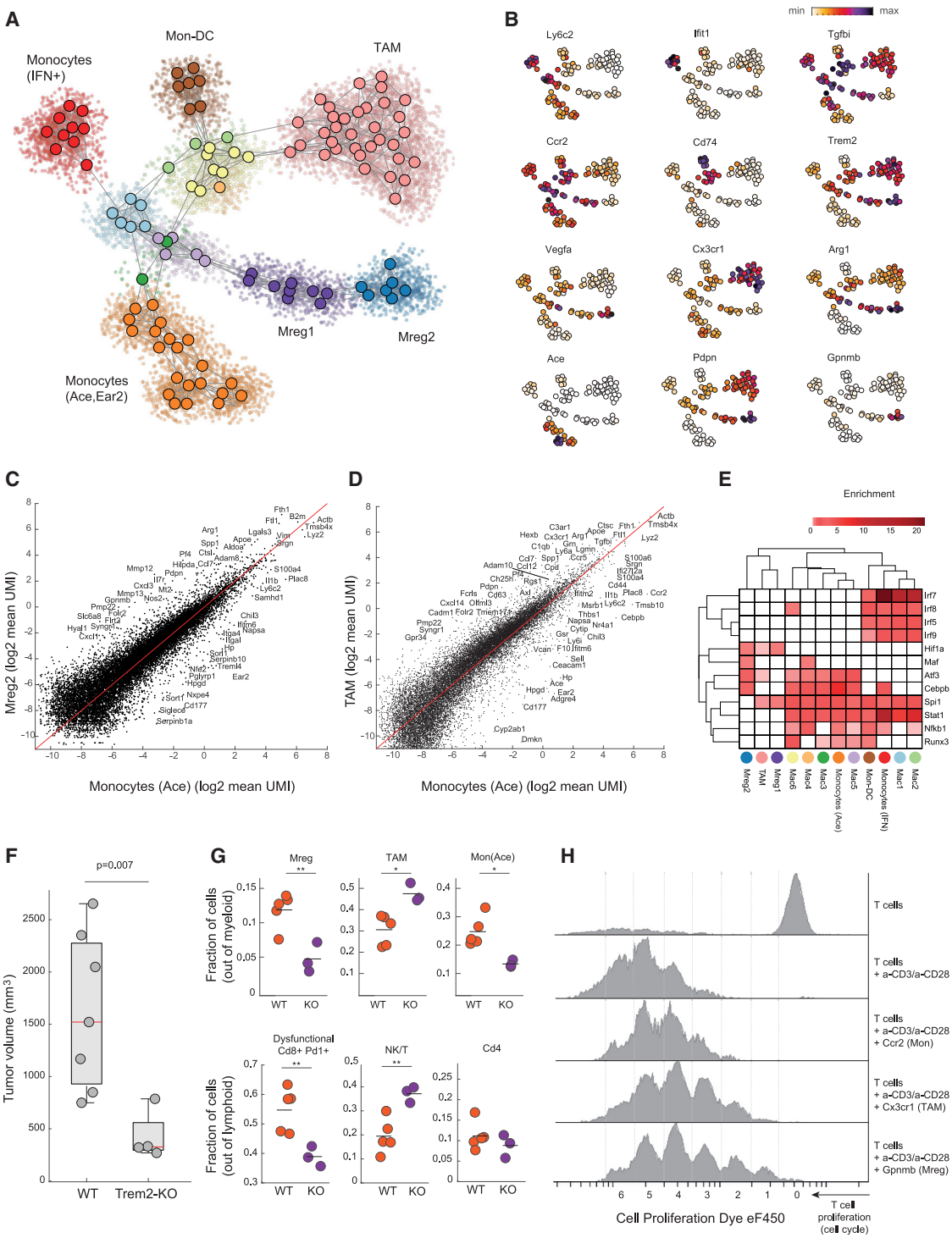

Figure 5. Trem2 Promotes T Cell Dysfunction and Tumor Immune Escape

(A) Two-dimensional graph projection of 115 metacells representing 1,2081 myeloid cells. Different colors represent different cell population, as indicated in the plot.

(B) Projection of key marker genes onto the graph plot.

(C) Scatterplot showing the mean UMI counts (log2 scale) of Mreg cells (y axis) compared with monocytes (Ace) (x axis).

(D) Scatterplot showing the mean UMI counts (log2 scale) of TAMs (y axis) compared with monocytes (Ace) (x axis).

(E) Heatmap showing enrichment of TF binding sites in the regulatory regions for each cluster. Only TFs with a significant normalized enrichment score (NES > 3.5) and mean expression above 0.1 UMI in the relevant cluster are shown.

(legend continued on next page)

T cell proliferation. This suggests that, at least in cell culture models, Trem2 plays an important role in regulation of immunosuppressive activity of myeloid cells.

To evaluate Trem2 activity *in vivo*, we compared MCA205 tumor growth in *Trem2*$^{+/+}$ (wild-type [WT]) and *Trem2*$^{-/-}$ mice and observed a significant reduction in tumor volume in *Trem2*$^{-/-}$ mice (Figures 5F and S7F). To further study the role of Trem2 on the intra-tumoral immune environment, we performed scRNA-seq of immune cells derived from MCA205-bearing mice from a *Trem2*$^{+/+}$ and *Trem2*$^{-/-}$ background, capturing a total of 15,808 QC-positive cells. Focusing on Trem2-expressing myeloid cells, we found a significant reduction in the Mreg cell population in the TME ($p = 0.0096$, two-sample t test) together with an increase in the TAM population in *Trem2*$^{-/-}$ mice compared with the WT (Figures 5G and S7B). Examination of the lymphoid compartment in WT and *Trem2*$^{-/-}$ mice revealed a notable decrease in CD8$^+$ dysfunctional T cells (expressing PD-1 and Tim-3) along with a significant expansion of the natural killer (NK) and cytotoxic T cell populations (Figure 5G; $p = 0.0085$, two-sample t test). To assess the functional effect of the different tumor-infiltrating myeloid populations on activated T lymphocyte proliferation, we used a T cell proliferation assay. Tumor-infiltrating myeloid populations (Mreg cells, TAMs, and Ccr2$^+$) were isolated, sorted by FACS, and co-cultured with cell proliferation dye-labeled splenic isolated naive CD8 T cells activated with α-CD3 and α-CD28. Although CD8$^+$ T cells co-cultured with intra-tumoral Ccr2$^+$ monocytes showed full proliferative behavior with no indication of suppression, we observed a considerable reduction in proliferation of activated CD8$^+$ T cells that were co-cultured with Cx3cr1$^+$ TAMs and an even more dominant suppression phenotype when cultured with Gpnmb$^+$ Mreg cells (Figures 5H and S7G). Our results demonstrate that Arg1$^+$ tumor-infiltrating myeloid cells contain two molecularly distinct myeloid populations: TAMs and Mreg cells. Trem2 knockout mice show that, although both populations are defined by Trem2 expression, only the Mreg cell populations are affected by Trem2 ablation. Altogether, we show that Trem2 deficiency leads to significant reduction in immunosuppression in a macrophage cell line and in the TME *in vivo*, which entails reactivation of the immune system, dramatically inhibiting tumor growth.

DISCUSSION

Although scRNA-seq technologies are major drivers in research and discovery, addition of other layers of cellular information, ranging from DNA to lineage, chromatin accessibility, surface protein expression, and perturbations, has recently had important effects on many fields, especially when these modalities are combined with the cellular transcriptome (Giladi and Amit, 2018; Stuart and Satija, 2019). Combining massively parallel scRNA-seq with intracellular protein measurements may enable capturing additional layers of information that have not been currently profiled at this resolution and scale, including TFs, signaling activity, and metabolism. Here, we developed a broadly applicable technology for profiling integrated single-cell transcriptional, signaling, TF, and metabolism maps (INs-seq).

We successfully applied INs-seq to investigate the molecular programs associated with distinct intracellular proteins and showed that our unique technology is applicable for single-cell profiling of diverse intracellular modalities ranging from TFs to signaling and metabolic pathways *in vitro* and *in vivo*. Our current focus of immune characterization is dependent on cell surface markers that outline cell lineages. The INs-seq technology enables us to investigate intracellular signals that may not be congruent with cell lineages and, hence, adds additional and important layers of signaling and metabolic pathways and shows their effect on immune function in diverse microenvironments. We profiled *in vitro* myeloid cells according to post-translational modification of the pp38 MAPK, a downstream signaling component of LPS TLR4 stimulation, and uncovered differential activation of DCs versus monocytes. We also demonstrate the potential of INs-seq to characterize novel immune cell populations based on single-cell profiling of TF circuits. So far, such efforts could only be approached using engineered TF reporter transgenic animal models, which have been an instrumental for discovery of novel immune populations. INs-seq T cell TF maps defined the interplay between TCF7 and ID2 in controlling the CD8 T cell cellular state and identified the molecular profile of effector and CM T cells in PBMC. Additionally, profiling of FOXP3$^+$ immune cells defined the unique molecular signature of Treg cells from different tissues, including tumor-resident and human blood Treg cells.

Finally, we analyzed suppressive metabolic circuits within the TME by direct targeting of Arg1$^+$ myeloid cells. We found two distinct populations of Arg1$^+$ Trem2$^+$ cells in tumor: a TAM population and a population of monocytic regulatory cells characterized by defined surface markers and signaling, including hypoxia. We further demonstrated the immunosuppressive activity of the Trem2$^+$ populations. Our findings identified Trem2 as a marker and important regulator of myeloid suppressive cells. Genetic ablation of Trem2 in mice led to a dramatic decrease in the Mreg cell population with an increase in immune reactivity toward the tumor, including a decrease in dysfunctional CD8$^+$ T cells and an increase in NK and cytotoxic T cells. Our results are starting to define the role of Trem2 in regulating the suppressive nature of myeloid cells in the TME. These results highlight

(F) MCA205 tumor volume (day 19) of WT and Trem2 knockout (KO) mice. Each point represents one animal; the red line represents mean volume. Error bars indicate mean ± SEM ($p = 0.007$, one-way ANOVA).

(G) Percentage of key cell populations in WT and Trem2 KO in the MCA205 TME (day 19). Each point represents one animal; the black line indicates average percentage. Stars mark a significant p value of a t test between the fraction of cells in the WT and Trem2 KO (Mreg cells, $p = 0.0068$; TAMs, $p = 0.0107$; Ace, $p = 0.011$; CD8$^+$Pd1$^+$, $p = 0.0096$; NK and/or T cells, $p = 0.0085$; one-way ANOVA).

(H) Flow cytometry histogram for T cell proliferation analysis showing the cell proliferation dye eFluor 450 fluorescence signal of WT splenic CD8 T cells stimulated with anti-CD3 and anti-CD28 and co-cultured for 48 h with MCA205 intra-tumoral CD11b$^+$ Ccr2$^+$ (Mon), Cx3cr1+ (TAMs), or Gpnmb$^+$ (Mreg cells).

See also Figure S7.

the potential of targeting Trem2 signaling as an effective strategy for reactivation of the immune response toward tumors.

Our experiments also highlight several remaining challenges in the current version of the INs-seq technology. First, combining a large number of intracellular markers will improve our ability to elucidate complete signaling and metabolic pathways. Because of the limited number of currently available fluorophores for FACS, it will be of importance to incorporate oligo-barcoded antibodies into our technology to quantitatively target dozens of proteins simultaneously. Second, although the cluster of differentiation (CD) extracellular markers were effectively developed and validated by the community for FACS analysis over many years, we are still missing such validated markers for intracellular proteins and PTM. Third, following INs-seq fixation, although the general number of RNA molecules is preserved, we still observe some RNA fragmentation, resulting in a lower median of molecules captured per cell in the scRNA-seq protocols. Reducing this fragmentation as well as including shorter molecules in the final single-cell library will further improve the quality of the INs-seq data.

Profiling cell populations within the framework of traditional cell lineages as defined by CD markers can potentially overlook important functional heterogeneity. Distinct lineages may share the same metabolic activities and signaling and, therefore, function in a coherent manner. Our application of INs-seq is not limited to classical cell markers; rather, this technology characterizes cellular states through the lens of TF profiles and intracellular signaling activity, bringing the potential of associating the epigenetic, signaling, and metabolic activity landscape onto the lineage manifold. This conceptual novelty of incorporating intracellular factors in addition to the transcriptome is also not restricted to the study of physiological behaviors of cells and tissues and may serve as an engine for analyzing perturbations, such as CRISPR genetic screens, drug or antibody screening, and their outcomes in different environments and pathologies. The robustness of INs-seq across a large variety of modalities and cells from different origins, including human clinical samples, demonstrates its potential to investigate a vast number of unresolved biological questions.

STAR★METHODS

Detailed methods are provided in the online version of this paper and include the following:

- KEY RESOURCES TABLE
- RESOURCE AVAILABILITY
  - Lead Contact
  - Materials Availability
  - Data and Code Availability
- EXPERIMENTAL MODEL AND SUBJECT DETAILS
  - Mice
  - Bone marrow derived cell culture
  - Tumor cell line
  - Human peripheral blood of healthy donors and Isolation of peripheral blood PBMC
- METHOD DETAILS
  - INs-seq fixation and intracellular staining protocol
  - 1- Cell surface staining
  - 2- INs-seq fixation
  - 3- Intracellular staining
  - Fixation and intracellular staining methods
  - 2 – Fixation methods
  - mRNA quality comparison between fixation methods using RT-qPCR
  - RT-qPCR for gene enrichment validation
  - Mouse spleenocytes sorting
  - Isolation of T-regulatory cells from mouse tumors and cervical lymph nodes
  - Tumor growth measurements
  - Isolation of tumor infiltrating leukocytes
  - Flow cytometry single cell sorting for Mars-seq 2.0
  - Mass Cytometry (CyTOF)
  - Flow cytometry bulk cell sorting for qPCR experiments
  - Droplet-based scRNA-seq (10x Chromium)
  - MARS-seq 2.0 library preparation
  - Suppression assay
  - Trem2 guide RNA cloning
  - Lentivirus production
  - Trem2 knockout N9 cell line generation
  - Western blot validation for Trem2 N9 cell line knock out
- QUANTIFICATION AND STATISTICAL ANALYSIS
  - Single cell RNA data processing (10x)
  - Chromium (10x) data integration and clustering analysis
  - MARS-seq processing
  - Metacell analysis
  - Statistical analysis

SUPPLEMENTAL INFORMATION

Supplemental Information can be found online at https://doi.org/10.1016/j.cell.2020.06.032.

ACKNOWLEDGMENTS

We thank Dr. A. Giladi and Dr. A. Deczkowska for reviewing the manuscript, N. David and T. Wiesel from the Scientific Illustration unit of the Weizmann Institute for artwork, Dr. M. Kedmi from the Advanced Sequencing Technologies unit, and members of the Amit laboratory for discussions. I.A. is an Eden and Steven Romick Professorial Chair and is supported by Merck KGaA (Darmstadt, Germany); the Chan Zuckerberg Initiative (CZI); an HHMI international scholar award; European Research Council Consolidator Grant (ERC-COG) 724471-HemTree2.0; an SCA award from the Wolfson Foundation and Family Charitable Trust; the Thompson Family Foundation; MRA Established Investigator Award 509044; D. Dan and Betty Kahn Foundation; the Ernest and Bonnie Beutler Research Program for Excellence in Genomic Medicine; the Helen and Martin Kimmel Award for Innovative Investigation; a NeuroMac DFG/Transregional Collaborative Research Center grant; International Progressive MS Alliance/NMSS PA-1604 08459; and an Adelis Foundation grant. F.S. is a recipient of the Israeli Council for Higher Education MSc and PhD fellowships.

AUTHOR CONTRIBUTIONS

Y.K. developed experimental protocol; designed, performed, and analyzed experiments; and wrote the manuscript. F.S. and A.Y. designed, performed, and analyzed experiments and wrote the manuscript. I.Y contributed to development of the experimental protocols. D.S. performed bioinformatic analyses. D.A.J. and H.K.-S. contributed to development of the experimental protocols. C.B., A.M., M.C., S.-Y.W., B.L., T.-M.S., and E.D. contributed to the

experiments. A.W. conceptualized, designed, and analyzed experiments; developed computational methods; performed bioinformatic analyses; and wrote the manuscript. I.A. developed experimental protocols, directed the project, conceptualized and designed experiments, interpreted results, and wrote the manuscript.

DECLARATION OF INTERESTS

A patent application has been filed related to this work.

Received: January 16, 2020
Revised: May 6, 2020
Accepted: June 19, 2020
Published: August 11, 2020

REFERENCES

Alles, J., Karaiskos, N., Praktiknjo, S.D., Grosswendt, S., Wahle, P., Ruffault, P.L., Ayoub, S., Schreyer, L., Boltengagen, A., Birchmeier, C., et al. (2017). Cell fixation and preservation for droplet-based single-cell transcriptomics. BMC Biol. *15*, 44.

Amit, I., Garber, M., Chevrier, N., Leite, A.P., Donner, Y., Eisenhaure, T., Guttman, M., Grenier, J.K., Li, W., Zuk, O., et al. (2009). Unbiased reconstruction of a mammalian transcriptional network mediating pathogen responses. Science *326*, 257–263.

Arlauckas, S.P., Garren, S.B., Garris, C.S., Kohler, R.H., Oh, J., Pittet, M.J., and Weissleder, R. (2018). Arg1 expression defines immunosuppressive subsets of tumor-associated macrophages. Theranostics *8*, 5842–5854.

Azizi, E., Carr, A.J., Plitas, G., Cornish, A.E., Konopacki, C., Prabhakaran, S., Nainys, J., Wu, K., Kiseliovas, V., Setty, M., et al. (2018). Single-Cell Map of Diverse Immune Phenotypes in the Breast Tumor Microenvironment. Cell *174*, 1293–1308.e36.

Baran, Y., Bercovich, A., Sebe-Pedros, A., Lubling, Y., Giladi, A., Chomsky, E., Meir, Z., Hoichman, M., Lifshitz, A., and Tanay, A. (2019). MetaCell: analysis of single-cell RNA-seq data using K-nn graph partitions. Genome Biol. *20*, 206.

Baron, C.S., Barve, A., Muraro, M.J., van der Linden, R., Dharmadhikari, G., Lyubimova, A., de Koning, E.J.P., and van Oudenaarden, A. (2019). Cell Type Purification by Single-Cell Transcriptome-Trained Sorting. Cell *179*, 527–542.e19.

Bronte, V., Serafini, P., Mazzoni, A., Segal, D.M., and Zanovello, P. (2003). L-arginine metabolism in myeloid cells controls T-lymphocyte functions. Trends Immunol. *24*, 302–306.

Caldwell, R.W., Rodriguez, P.C., Toque, H.A., Priya Narayanan, S., and Caldwell, R.B. (2018). Arginase: A multifaceted enzyme important in health and disease. Physiol. Rev. *98*, 641–665.

Cannarile, M.A., Lind, N.A., Rivera, R., Sheridan, A.D., Camfield, K.A., Wu, B.B., Cheung, K.P., Ding, Z., and Goldrath, A.W. (2006). Transcriptional regulator Id2 mediates CD8+ T cell immunity. Nat. Immunol. *7*, 1317–1325.

Cao, X., Cai, S.F., Fehniger, T.A., Song, J., Collins, L.I., Piwnica-Worms, D.R., and Ley, T.J. (2007). Granzyme B and perforin are important for regulatory T cell-mediated suppression of tumor clearance. Immunity *27*, 635–646.

Chen, X., and Oppenheim, J.J. (2011). Resolving the identity myth: Key markers of functional CD4 +FoxP3 + regulatory T cells. Int. Immunopharmacol. *11*, 1489–1496.

Deczkowska, A., Weiner, A., and Amit, I. (2020). The Physiology, Pathology, and Potential Therapeutic Applications of the TREM2 Signaling Pathway. Cell *181*, 1207–1217.

Gabrilovich, D.I. (2017). Myeloid-derived suppressor cells. Cancer Immunol. Res. *5*, 3–8.

Gabrilovich, D.I., and Nagaraj, S. (2009). Myeloid-derived suppressor cells as regulators of the immune system. Nat. Rev. Immunol. *9*, 162–174.

Gerlach, J.P., van Buggenum, J.A.G., Tanis, S.E.J., Hogeweg, M., Heuts, B.M.H., Muraro, M.J., Elze, L., Rivello, F., Rakszewska, A., van Oudenaarden, A., et al. (2019). Combined quantification of intracellular (phospho-)proteins and transcriptomics from fixed single cells. Sci. Rep. *9*, 1469.

Gervois, P., and Lambrichts, I. (2019). The emerging role of triggering receptor expressed on myeloid cells 2 as a target for immunomodulation in ischemic stroke. Front. Immunol. *10*, 1668.

Giladi, A., and Amit, I. (2018). Single-Cell Genomics: A Stepping Stone for Future Immunology Discoveries. Cell *172*, 14–21.

Glass, C.K., and Natoli, G. (2016). Molecular control of activation and priming in macrophages. Nat. Immunol. *17*, 26–33.

Griffiths, J.A., Scialdone, A., and Marioni, J.C. (2018). Using single-cell genomics to understand developmental processes and cell fate decisions. Mol. Syst. Biol. *14*, e8046.

Held, W., Siddiqui, I., Schaeuble, K., and Speiser, D.E. (2019). Intratumoral CD8$^+$ T cells with stem cell-like properties: Implications for cancer immunotherapy. Sci. Transl. Med. *11*, eaay6863.

Helft, J., Böttcher, J., Chakravarty, P., Zelenay, S., Huotari, J., Schraml, B.U., Goubau, D., and Reis e Sousa, C. (2015). GM-CSF Mouse Bone Marrow Cultures Comprise a Heterogeneous Population of CD11c(+)MHCII(+) Macrophages and Dendritic Cells. Immunity *42*, 1197–1211.

Im, S.J., Hashimoto, M., Gerner, M.Y., Lee, J., Kissick, H.T., Burger, M.C., Shan, Q., Hale, J.S., Lee, J., Nasti, T.H., et al. (2016). Defining CD8+ T cells that provide the proliferative burst after PD-1 therapy. Nature *537*, 417–421.

Jaitin, D.A., Kenigsberg, E., Keren-Shaul, H., Elefant, N., Paul, F., Zaretsky, I., Mildner, A., Cohen, N., Jung, S., Tanay, A., and Amit, I. (2014). Massively parallel single-cell RNA-seq for marker-free decomposition of tissues into cell types. Science *343*, 776–779.

Jaitin, D.A., Weiner, A., Yofe, I., Lara-Astiaso, D., Keren-Shaul, H., David, E., Salame, T.M., Tanay, A., van Oudenaarden, A., and Amit, I. (2016). Dissecting Immune Circuits by Linking CRISPR-Pooled Screens with Single-Cell RNA-Seq. Cell *167*, 1883–1896.e15.

Jaitin, D.A., Adlung, L., Thaiss, C.A., Weiner, A., Li, B., Descamps, H., Lundgren, P., Bleriot, C., Liu, Z., Deczkowska, A., et al. (2019). Lipid-Associated Macrophages Control Metabolic Homeostasis in a Trem2-Dependent Manner. Cell *178*, 686–698.e14.

Josefowicz, S.Z., and Rudensky, A. (2009). Control of Regulatory T Cell Lineage Commitment and Maintenance. Immunity *30*, 616–625.

Kanton, S., Boyle, M.J., He, Z., Santel, M., Weigert, A., Sanchís-Calleja, F., Guijarro, P., Sidow, L., Fleck, J.S., Han, D., et al. (2019). Organoid single-cell genomic atlas uncovers human-specific features of brain development. Nature *574*, 418–422.

Keren-Shaul, H., Kenigsberg, E., Jaitin, D.A., David, E., Paul, F., Tanay, A., and Amit, I. (2019). MARS-seq2.0: an experimental and analytical pipeline for indexed sorting combined with single-cell RNA sequencing. Nature Protocols *14*, 1841–1862.

Keren-Shaul, H., Spinrad, A., Weiner, A., Matcovitch-Natan, O., Dvir-Szternfeld, R., Ulland, T.K., David, E., Baruch, K., Lara-Astaiso, D., Toth, B., et al. (2017). A Unique Microglia Type Associated with Restricting Development of Alzheimer's Disease. Cell *169*, 1276–1290.e17.

Kim, J.M., and Rudensky, A. (2006). The role of the transcription factor Foxp3 in the development of regulatory T cells. Immunol. Rev. *212*, 86–98.

Klages, N., Zufferey, R., and Trono, D. (2000). A stable system for the high-titer production of multiply attenuated lentiviral vectors. Mol. Ther. *2*, 170–176.

Kratchmarov, R., Magun, A.M., and Reiner, S.L. (2018). TCF1 expression marks self-renewing human CD8$^+$ T cells. Blood Adv. *2*, 1685–1690.

Kumar, H., Kawai, T., and Akira, S. (2011). Pathogen recognition by the innate immune system. Int. Rev. Immunol. *30*, 16–34.

Kumar, V., Patel, S., Tcyganov, E., and Gabrilovich, D.I. (2016). The Nature of Myeloid-Derived Suppressor Cells in the Tumor Microenvironment. Trends Immunol. *37*, 208–220.

Linde, N., Casanova-Acebes, M., Sosa, M.S., Mortha, A., Rahman, A., Farias, E., Harper, K., Tardio, E., Reyes Torres, I., Jones, J., et al. (2018). Macrophages

orchestrate breast cancer early dissemination and metastasis. Nat. Commun. *9*, 21.

Magnuson, A.M., Kiner, E., Ergun, A., Park, J.S., Asinovski, N., Ortiz-Lopez, A., Kilcoyne, A., Paoluzzi-Tomada, E., Weissleder, R., Mathis, D., and Benoist, C. (2018). Identification and validation of a tumor-infiltrating Treg transcriptional signature conserved across species and tumor types. Proc. Natl. Acad. Sci. USA *115*, E10672–E10681.

Masson, F., Minnich, M., Olshansky, M., Bilic, I., Mount, A.M., Kallies, A., Speed, T.P., Busslinger, M., Nutt, S.L., and Belz, G.T. (2013). Id2-mediated inhibition of E2A represses memory CD8+ T cell differentiation. J. Immunol. *190*, 4585–4594.

Murphy, T.L., Grajales-Reyes, G.E., Wu, X., Tussiwand, R., Briseño, C.G., Iwata, A., Kretzer, N.M., Durai, V., and Murphy, K.M. (2016). Transcriptional Control of Dendritic Cell Development. Annu. Rev. Immunol. *34*, 93–119.

Paul, F., Arkin, Y., Giladi, A., Jaitin, D.A., Kenigsberg, E., Keren-Shaul, H., Winter, D., Lara-Astiaso, D., Gury, M., Weiner, A., et al. (2015). Transcriptional Heterogeneity and Lineage Commitment in Myeloid Progenitors. Cell *163*, 1663–1677.

Peterson, V.M., Zhang, K.X., Kumar, N., Wong, J., Li, L., Wilson, D.C., Moore, R., McClanahan, T.K., Sadekova, S., and Klappenbach, J.A. (2017). Multiplexed quantification of proteins and transcripts in single cells. Nat. Biotechnol. *35*, 936–939.

Ricardo Miragaia, A.J., Gomes, T., Chomka, A., Haniffa, M., Powrie, F., and Teichmann Correspondence, S.A. (2019). Single-Cell Transcriptomics of Regulatory T Cells Reveals Trajectories of Tissue Adaptation. Immunity *50*, 493–504.e7.

Schaum, N., Karkanias, J., Neff, N.F., May, A.P., Quake, S.R., Wyss-Coray, T., Darmanis, S., Batson, J., Botvinnik, O., Chen, M.B., et al.; Tabula Muris Consortium; Overall coordination; Logistical coordination; Organ collection and processing; Library preparation and sequencing; Computational data analysis; Cell type annotation; Writing group; Supplemental text writing group; Principal investigators (2018). Single-cell transcriptomics of 20 mouse organs creates a Tabula Muris. Nature *562*, 367–372.

Schlepckow, K., Monroe, K.M., Kleinberger, G., Cantuti-Castelvetri, L., Parhizkar, S., Xia, D., Willem, M., Werner, G., Pettkus, N., Brunner, B., et al. (2020). Enhancing protective microglial activities with a dual function TREM2 antibody to the stalk region. EMBO Mol. Med. *12*, e11227.

Segerstolpe, Å., Palasantza, A., Eliasson, P., Andersson, E.M., Andréasson, A.C., Sun, X., Picelli, S., Sabirsh, A., Clausen, M., Bjursell, M.K., et al. (2016). Single-Cell Transcriptome Profiling of Human Pancreatic Islets in Health and Type 2 Diabetes. Cell Metab. *24*, 593–607.

Shah, D.K., and Zúñiga-Pflücker, J.C. (2014). An overview of the intrathymic intricacies of T cell development. J. Immunol. *192*, 4017–4023.

Stoeckius, M., Hafemeister, C., Stephenson, W., Houck-Loomis, B., Chattopadhyay, P.K., Swerdlow, H., Satija, R., and Smibert, P. (2017). Simultaneous epitope and transcriptome measurement in single cells. Nat. Methods *14*, 865–868.

Stuart, T., and Satija, R. (2019). Integrative single-cell analysis. Nat. Rev. Genet. *20*, 257–272.

Stuart, T., Butler, A., Hoffman, P., Hafemeister, C., Papalexi, E., Mauck, W.M., 3rd, Hao, Y., Stoeckius, M., Smibert, P., and Satija, R. (2019). Comprehensive Integration of Single-Cell Data. Cell *177*, 1888–1902.e21.

Tang, W., Lv, B., Yang, B., Chen, Y., Yuan, F., Ma, L., Chen, S., Zhang, S., and Xia, J. (2019). TREM2 acts as a tumor suppressor in hepatocellular carcinoma by targeting the PI3K/Akt/β-catenin pathway. Oncogenesis *8*, 9.

Togashi, Y., Shitara, K., and Nishikawa, H. (2019). Regulatory T cells in cancer immunosuppression - implications for anticancer therapy. Nat. Rev. Clin. Oncol. *16*, 356–371.

Tong, A.A., Forestell, B., Murphy, D.V., Nair, A., Allen, F., Myers, J., Klauschen, F., Shen, C., Gopal, A.A., Huang, A.Y., and Mandl, J.N. (2019). Regulatory T cells differ from conventional $CD4^+$ T cells in their recirculatory behavior and lymph node transit times. Immunol. Cell Biol. *97*, 787–798.

Turnbull, I.R., Gilfillan, S., Cella, M., Aoshi, T., Miller, M., Piccio, L., Hernandez, M., and Colonna, M. (2006). Cutting edge: TREM-2 attenuates macrophage activation. J. Immunol. *177*, 3520–3524.

Ulland, T.K., and Colonna, M. (2018). TREM2 — a key player in microglial biology and Alzheimer disease. Nat. Rev. Neurol. *14*, 667–675.

Veglia, F., Perego, M., and Gabrilovich, D. (2018). Myeloid-derived suppressor cells coming of age. Nat. Immunol. *19*, 108–119.

Willinger, T., Freeman, T., Herbert, M., Hasegawa, H., McMichael, A.J., and Callan, M.F.C. (2006). Human naive CD8 T cells down-regulate expression of the WNT pathway transcription factors lymphoid enhancer binding factor 1 and transcription factor 7 (T cell factor-1) following antigen encounter in vitro and in vivo. J. Immunol. *176*, 1439–1446.

Yamada, H., Maruo, R., Watanabe, M., Hidaka, Y., Iwatani, Y., and Takano, T. (2010). Messenger RNA quantification after fluorescence activated cell sorting using intracellular antigens. Biochem. Biophys. Res. Commun. *397*, 425–428.

Yang, C.Y., Best, J.A., Knell, J., Yang, E., Sheridan, A.D., Jesionek, A.K., Li, H.S., Rivera, R.R., Lind, K.C., D'Cruz, L.M., et al. (2011). The transcriptional regulators Id2 and Id3 control the formation of distinct memory CD8+ T cell subsets. Nat. Immunol. *12*, 1221–1229.

Zanoni, I., Ostuni, R., Marek, L.R., Barresi, S., Barbalat, R., Barton, G.M., Granucci, F., and Kagan, J.C. (2011). CD14 controls the LPS-induced endocytosis of Toll-like receptor 4. Cell *147*, 868–880.

Zeisel, A., Hochgerner, H., Lönnerberg, P., Johnsson, A., Memic, F., van der Zwan, J., Häring, M., Braun, E., Borm, L.E., La Manno, G., et al. (2018). Molecular Architecture of the Mouse Nervous System. Cell *174*, 999–1014.e22.

Zhang, X., Wang, W., Li, P., Wang, X., and Ni, K. (2018). High TREM2 expression correlates with poor prognosis in gastric cancer. Hum. Pathol. *72*, 91–99.

Zheng, H., Cheng, B., Li, Y., Li, X., Chen, X., and Zhang, Y.W. (2018). TREM2 in Alzheimer's Disease: Microglial Survival and Energy Metabolism. Front. Aging Neurosci. *10*, 395.

Zhong, L., Chen, X.F., Wang, T., Wang, Z., Liao, C., Wang, Z., Huang, R., Wang, D., Li, X., Wu, L., et al. (2017). Soluble TREM2 induces inflammatory responses and enhances microglial survival. J. Exp. Med. *214*, 597–607.

Zhou, X., Yu, S., Zhao, D.M., Harty, J.T., Badovinac, V.P., and Xue, H.H. (2010). Differentiation and persistence of memory CD8(+) T cells depend on T cell factor 1. Immunity *33*, 229–240.

STAR★METHODS

KEY RESOURCES TABLE

REAGENT or RESOURCE	SOURCE	IDENTIFIER
Antibodies		
APC-conjugated CD45	eBioscience	Cat#17-0451-82; AB_469392
EF450-conjugated CD11c	eBioscience	Cat#48-0114-82; AB_1548654
EF450-conjugated CD11b	eBioscience	Cat#48-0112-82; AB_1582236
FITC-conjugated Ly-6g	Biolegend	Cat#127605; AB_1236488
PE-conjugated Ly-6c	eBioscience	Cat#128007; AB_1186133
PE/cy7-conjugated CD14	Biolegend	Cat#123315; AB_10641133
FITC-conjugated MHCC-II (IA/I-E)	Biolegend	Cat#107606; AB_313321
Percp/cy5.5-conjugated CD11b	Biolegend	Cat#101228; AB_893232
FITC-conjugated TCR-b	Biolegend	Cat#109205; AB_313428
BV605-conjugated CD3	BD Bioscience	Cat#563219; AB_2738076
Pacific Blue-conjugated CD45	Cytognos	Cat#CYT-45PBZ
BV711-conjugated Cx3cr1	Biolegend	Cat#140931
PE-conjugated Ccr2	Biolegend	Cat#150609; AB_2616981
AF488-conjugated Pdpn	Biolegend	Cat#127405; AB_1133992
APC-conjugated Pdpn	Biolegend	Cat#127409; AB_10612940
EF660-conjugated Gpnmb	eBioscience	Cat#50-5708-80; AB_2574238
Percp/cy5.5-conjugated Il7r	eBioscience	Cat#45-1271-80; AB_906212
APC-conjugated pP38	eBioscience	Cat#17-9078-42
APC-conjugated Arg1	R&D Systems	Cat#IC5868A; AB_2810265
AF488-conjugated Foxp3	Biolegend	Cat#320011; AB_439747
Super bright780-conjugated CD19	eBioscience	Cat#78-0198-42; AB_2724070
Pacific Blue-conjugated CD16	Biolegend	Cat#302032; AB_2104003
FITC-conjugated CD3	Beckman Coulter	Cat#A07746; AB_2801270
APC/H7-conjugated CD8	BD Bioscience	Cat#560179; AB_1645481
APC-conjugated CD4	BD Bioscience	Cat#555349; AB_398593
PE-conjugated CD56	Cytognos	Cat#CYT-56PE; AB_2732847
EF450 -conjugated ID2	eBioscience	Cat#48-9475-82; AB_2735053
AF488-conjugated TCF7	Cell signaling	Cat#6444S; AB_2797627
141Pr-conjugated Ly-6G/C	FLUIDIGM	Cat#3141008B; AB_2814678
142Nd-conjugated CD11c	FLUIDIGM	Cat#3142003; AB_2814737
148Nd-conjugated CD11b	FLUIDIGM	Cat#3148003; AB_2814738
150Nd-conjugated Ly-6C	FLUIDIGM	Cat#3150010B
159Tb-conjugated CD279	FLUIDIGM	Cat#3159006
151Eu-conjugated CD25	FLUIDIGM	Cat#3151007; AB_2827880
156Gd-conjugated CD14	FLUIDIGM	Cat#3156009; AB_2814681
153Eu-conjugated CD274	FLUIDIGM	Cat#3153016B; AB_2687837
164Dy-conjugated Cx3cr1	FLUIDIGM	Cat#3164023; AB_2832247
168Er-conjugated CD8a	FLUIDIGM	Cat#3168003; AB_2811241
169Tm-conjugated CD206	FLUIDIGM	Cat#3169021B; AB_2832249
171Yb-conjugated CD44	FLUIDIGM	Cat#3171003
172Yb-conjugated CD4	FLUIDIGM	Cat#3172003; AB_2811242
176Yb-conjugated anti-cross APC	FLUIDIGM	Cat#3176007; AB_2811236
89Y-conjugated CD45	FLUIDIGM	Cat#3089005; AB_2651152

(*Continued on next page*)

Continued

REAGENT or RESOURCE	SOURCE	IDENTIFIER
143Nd-conjugated TCR-b	FLUIDIGM	Cat#3143010
209Bi-conjugated I-A/I-E	FLUIDIGM	Cat#320900B
Purified Trem2	R&D Systems	Cat#MAB17291-100
Trem2 antibody	Abcam	Cat#Ab86491; AB_1925525
Purified Podoplanin (Pdpn)	Biolegend	Cat#127402; B_1089187
Chemicals, Peptides, Enzymes, and Recombinant Proteins		
DTT	Sigma-Adrich	Cat#43816
Pierce Saturated Ammonium Sulfate	Sigma-Adrich	Cat#45216
Albumin Bovine, Fraction V	MP-Biomedicals	Cat#9048-46-8
Collagenase IV	Worthington	Cat#LS004188
DNase	Sigma-Adrich	Cat#11284932001
Ficoll-Paque PLUS	Sigma-Aldrich	Cat#17-1440-03
LPS EK Ultrapure	Invivogen	tlrl-peklps
Red blood lysis buffer	Sigma-Aldrich	R7757
16% Formaldehyde	Sigma-Aldrich	Cat#28906
Methanol absolute	Bio-Lab	NA
EDTA	Sigma	Cat#03690
Pierce Protein-Free (PBS) Blocking Buffer	Thermo Fisher	Cat#37584
GM-CSF	PeproTech	Cat#315-03
Rm IL-2	R&D Systems	Cat#402-ML
Sodium Chloride 5M	Sigma-Adrich	Cat#5150
Sodium phosphate monobasic monohydrate	Sigma-Adrich	Cat#3522
FastDigest ESP3I	Thermo Fisher	FD0454
LentiCas9-BLAST	Addgene	Plasmid #52962
Sodium Phosphate Dibasic	Sigma-Adrich	Cat#9390
Critical Commercial Assays		
CD3/CD28 expansion kit	Sigma-Aldrich	Cat#11452D
CD45 microbeads	Milteny Biotech	Cat#130-045-801
CD8a microbeads	Milteny Biotech	Cat#130-095-236
Cell Proliferation Dye eFluor 450	Thermo Fisher	Cat#65-0482-85
Recombinant human TGF-beta1	Peprotech	Cat#100-21C-50
True-Nuclear Transcription Factor Buffer Set	Biolegend	Cat#424401
Dynabeads mRNA DIRECT Purification Kit	Invitrogen	Cat# 61012
Lightning-Link® Metal Labeling Kit	Expedeon	Cat#M139-0010
Maxpar PBS	FLUIDIGM	Cat#201058
Maxpar Cell staining buffer	FLUIDIGM	Cat#201068
Maxper Nuclear Antigen Stainig perm (1X)	FLUIDIGM	Cat#S00110
Maxper Nuclear Antigen Staining Buffer Diluent	FLUIDIGM	Cat#S00109
Maxper Nuclear Antigen Staining Buffer Concentrate (4X)	FLUIDIGM	Cat#Soo108
Deposited Data		
Raw data files for single-cell RNA-seq	NCBI Gene Expression Omnibus	GEO: GSE150877
Experimental Models: Organisms/Strains		
Mouse: C57BL/6 WT	Harlan	N/A
Mouse: Trem2$^{-/-}$	Generated in the Laboratory of Prof. Marco Colonna	N/A
Mouse: Foxp3-RFP (Tg(Foxp3-RFP,-cre))	Generated in the Laboratory of Dr. Jakub Abramson	

(*Continued on next page*)

Continued

REAGENT or RESOURCE	SOURCE	IDENTIFIER
Experimental Models: Cell Lines		
MCA-205	Provided by the Laboratory of Sergio Quezada	N/A
Oligonucleotides		
Primers for qPCR, see Table S7	This paper	N/A
Software and Algorithms		
MATLAB	Math Works	https://www.mathworks.com/
R 3.5.0	The R Foundation	http://www.r-project.org/
FlowJo software	FlowJo, LLC	https://www.flowjo.com/
Other		
MARS-seq reagents	Jaitin et al., 2014; Keren-Shaul et al., 2019	N/A

RESOURCE AVAILABILITY

Lead Contact

Further information and requests for reagents should be directed to and will be fulfilled by lead author Ido Amit (ido.amit@weizmann.ac.il).

Materials Availability

This study did not generate new unique reagents.

Data and Code Availability

The accession number for the processed data reported in this paper is NCBI GEO: GSE150877. Scripts reproducing the analysis are available at: https://bitbucket.org/amitlab/.

EXPERIMENTAL MODEL AND SUBJECT DETAILS

Mice

Wild-type (WT) mice (8 weeks, females, C57BL/6) were purchased from Harlan and housed in the Weizmann Institute animal facility. Trem2$^{-/-}$ knock-out (KO) mice (8 weeks, females) were kindly provided by Prof. Marco Colonna (Turnbull et al., 2006). Foxp3-RFP (Tg(Foxp3-RFP,-cre)) mice were kindly provided by Dr. Jakub Abramsaon (10 weeks, females). Mice were provided with food and water *ad libitum* and housed under a strict 12 hr light-dark cycle. All experimental procedures were approved by the Institutional Animal Care and Use Committee (IACUC).

Bone marrow derived cell culture

8 weeks female C57BL/6 mice were sacrificed by cervical dislocation. To isolate the bone marrow, femora and tibiae from one leg were removed, cleaned from flesh, and flushed with C10 culture medium (RPMI-1640 supplemented with 15% serum, 1% x100 non-essential amino acids, 10mM HEPES buffer, 1mM sodium pyruvate, 2mM L-glutamine, and 50 μM b-mercaptoethanol) using a G21 needle syringe. Flushed bone marrow was filtered through a 70-μm cell strainer and spun down in a cold centrifuge at 300xg for 5 min. Cells were re-suspended in 250 μL RBC lysis solution (Sigma) per leg and incubated for 5 min at room temperature, washed, and resuspended in pre-warmed C10 medium. Cultures were set by plating 2x10^6 cells in 10mL C10 supplemented with 20 ng/ml GM-CSF in a 100 mm non-tissue culture plate, and incubated under standard culture conditions (37°C, 5% CO2) (Day 0). On day 2 another 10 mL C10 medium supplemented with 20 ng/ml GM-CSF was added. On day 5, three quarter of the medium was replaced with fresh C10 medium supplemented with 20 ng/ml GM-CSF. On day 7, another 5 mL of C10 medium supplemented with 10 ng/ml GM-CSF. On day 8, non-adherent and loosely adherent cells in the culture supernatant were harvested by gentle washing and re-cultured in a fresh C10 medium supplemented with 10 ng/ml GM-CSF in new non-tissue culture plates and used as starting material for all BMDC experiments.

Tumor cell line

MCA-205 fibrosarcoma cell lines were kindly provided by Sergio Quezada group at UCL cancer institute, London, UK. Cells were cultured in DMEM (41965-039) medium supplemented with 10% heat-inactivated FBS, 1mM sodium pyruvate, 2mM l-glutamine,

1% penicillin-streptomycin (Thermo Fisher Scientific). Cells were cultured in 100 mm tissue culture plates in an incubator with humidified air and 5% CO2 at 37°C. Cell lines were validated for lack of mycoplasma infection using primers for mycoplasma-specific 16S rRNA gene region (EZPCR Mycoplasma Kit; Biological Industries).

Human peripheral blood of healthy donors and Isolation of peripheral blood PBMC

Blood was taken from 3 healthy peripheral blood donors (Donor 1: male, 32; Donor 2: male, 33; Donor 3: male, 26). The peripheral blood collecting samples is part of the (0220-15-TLV) approval. PBMCs were purified from fresh blood samples by sterile density gradient separation by density centrifugation media (Ficoll-Paque (GE Healthcare Life Sciences)) in a 1:1 ratio. Centrifugation (460 g, 25 min,) was performed at 10°C, and the mononuclear cells were carefully aspirated and washed with ice-cold FACS buffer, followed by red blood lysis (Sigma-Aldrich) for 5 min at 4°C and washing with ice cold FACS buffer.

METHOD DETAILS

INs-seq fixation and intracellular staining protocol

Recommended fluorophores to use for both extracellular and intracellular staining with INs-seq protocol: Af488, Af647, ef450, ef660, APC, FITC, Pacific blue, BV711.

1- Cell surface staining

Cells or tissue from *in vitro* and *in vivo* experiments respectively were dissociated into single cell suspension and washed with 10 mL cold PBS. Cells were stained in ice cold washing buffer (−/− Dulbecco's Phosphate Buffered Saline (Biological industries), 0.5% BSA (MP-Biomedicals), 2mM EDTA (Merck) with fluorophores conjugated antibodies (final concentration of 5 μg/mL) on ice for 30 minutes in the dark.

2- INs-seq fixation

Surface-stained cells were washed in 10 mL washing buffer and centrifuged at 400 g for 5 minutes. Cell pellet ($1x10^6$ – $5x10^6$ cells) was resuspended in 1 volume (100 μl) of cold PBS (0.4U/μL RNasin® Plus RNase Inhibitor (Promega)). Cell suspension was fixed with 9 volumes (900 μl) of cold 100% methanol (Bio-Lab) (pre-chilled to −20°C) for 10 minutes on ice in the dark. To avoid cell clumping, methanol was added in drops, while gently vortexing the cell suspension.

Fixed cells were pelleted at 900 g for 3 minutes right after fixation. Methanol-PBS solution was completely discarded. Cell pellet was washed (not resuspended) twice with ice-cold PBS (0.4U/μL RNasin® Plus RNase Inhibitor) without breaking the pellet, for complete removal of methanol leftovers. Cell pellet was resuspended in 100 μL of enzyme blocking buffer containing ammonium sulfate (Thermo Fisher) solution (0.05M EDTA (Sigma), 0.8U/μL RNasin® Plus RNase Inhibitor, pH of 5.2) and kept on ice for 10 minutes in the dark.

3- Intracellular staining

To wash enzyme blocking buffer solution, 1 mL washing buffer (0.4U/μL RNasin® Plus RNase inhibitor) was added, cells then were pelleted at 900 g for 3 minutes. To completely remove enzyme blocking buffer, cell pellet was washed twice with ice-cold washing buffer (0.4U/μL RNasin® Plus RNase inhibitor) without re-suspension. Cell pellet was then incubated in the dark for 20 minutes with 100 μl intracellular staining buffer (−/− Dulbecco's Phosphate Buffered Saline (Biological industries), 0.5% BSA (MP biochemical), 2M EDTA (Sigma) with the desired intracellular antibody). At the end of the incubation, 1 mL washing buffer (0.4U/μL RNasin® Plus RNase inhibitor) was added on top of the 100 μl intracellular staining buffer, cells were pelleted at 900 g for 3 minutes. Cell pellet was resuspended in 1 mL preservation buffer, filtered with 70 um nylon mesh and kept on ice until cell sorting.

Fixation and intracellular staining methods

1- Cell surface staining

Cells or tissue from *in vitro* and *in vivo* experiments respectively were dissociated into single cell suspension and washed with 10 mL cold PBS. Cells were stained in ice cold washing buffer (−/− Dulbecco's Phosphate Buffered Saline (Biological industries), 0.5% BSA (MP-Biomedicals), 2mM EDTA (Merck)) with fluorophores conjugated antibodies (final concentration of 5 μg/mL) on ice for 30 minutes in the dark.

2 – Fixation methods

Methanol based cell fixation protocol: adopted from Alles et al. (2017). Surface-stained cells were washed in 10 mL washing buffer and centrifuged at 400 g for 5 minutes. Cells were handled in regular microcentrifuge tubes to minimize cell loss and kept cold at all times. Cells were resuspended in 100 μL of ice-cold PBS. To avoid cell clumping, 9 volumes (900 μl) of methanol (pre-chilled to –20°C) were added dropwise, while gently mixing or vortexing the cell suspension (final concentration: 90% methanol in PBS). The methanol-fixed cells were kept on ice for a minimum of 15 min. For rehydration, cells were pelleted at 900 g for 4 min, rehydrated in PBS (0.01% BSA, 1U/μl RNasin® Plus RNase inhibitor) pelleted, centrifuged, resuspended again in PBS (0.01% BSA, 1U/μl RNase inhibitor) and filtered with 70 um nylon mesh and kept on ice until cell sorting.

PFA based – Surface-strained cells were washed in 10 mL washing buffer and centrifuged at 400 g for 5 minutes. True-Nuclear Transcription Factor Buffer Set commercial kit was used according to the published protocol. Cells were filtered with 70 um nylon mesh and kept on ice until cell sorting.

DSP based cell fixation protocol: was adopted from Gerlach et al. (2019). Surface-srained cells were washed in 10 mL washing buffer and centrifuged at 400 g for 5 minutes. Cells were fixed using a combination of 2.5 mM DSP (Thermo Scientific) and 2.5 mM SPDP (Thermo Scientific) in DMSO for 45 minutes in 200 mM Sodium Phosphate Buffered Saline pH 8.4 (1M stock solution of Sodium-Phosphate buffer includes 1M NaH2PO4 (Sodium phosphate monobasic (Sigma) and 1M Na2HPO4 (Sodium phosphate dibasic (Sigma)) solutions), and 150mM NaCl (Sigma). After fixative quenching with 100 mM Tris-HCl pH 7.5, 150 mM NaCl the cells were blocked and permeabilized using 0.5X Protein Free Blocking Buffer (PFBB, Thermo Scientific) in PBS, 0.5 U/μl RNasin® Plus RNase and 0.1% Triton X-100. Next, cells were stained overnight with 0.5 X PFBB in PBS containing 2 U/μl RNasin® Plus RNase inhibitor, 0.1% Triton and 250 ng/μl of the desired intracellular antibody. After staining, the cells were gently washed 6 times with 10 ml 0.1X PFBB in PBS, filtered with 70 um nylon mesh and kept on ice until cell sorting.

mRNA quality comparison between fixation methods using RT-qPCR

Day 9 culture BMDCs were fixed according to the different fixation protocol guidelines including INS-seq (as described above), and stained for Cd11c. 5000 cells from each protocol were sorted directly into 40 μl of lysis binding buffer (Invitrogen). mRNA was captured with 12 μL of Dynabeads oligo(dT) (Invitrogen) according to manufacturer protocol. For DSP samples only, mRNA was reverse cross-linked by incubation with 6 mM dNTP, 150 mM Tris pH 8, 90 mM DTT, 0.1% Triton, 6 U/μl RNAsin Plus for 45 minutes at 25 °C, followed by 5 minutes at 65 °C and then cooled to 4 °C. For all fixation protocols each half of the mRNA material was either reverse transcribed or reverse transcribed and amplified (14 cycles) in the same reaction (RT-PCR). cDNA or amplified cDNA were diluted (1:40) and quantified in qPCR using mouse Actb primers.

RT-qPCR for gene enrichment validation

mRNA from cells sorted in to lysis/binding buffer was captured with 12 μL of Dynabeads oligo(dT) (Invitrogen), washed, and eluted at 85°C with 10 μL of 10 mM Tris-HCl (pH 7.5). mRNA was reverse transcribed using SuperScript II (ThermoFisher) and cDNA was diluted 1:40 for qPCR measurement using the different genes primers (See Table S7).

Mouse spleenocytes sorting

Spleen was harvested from 8 weeks' females C57BL/6 mice, mashed through 100uM cell strainer and washed with ice-cold MACS buffer. cells were centrifuged at 300 g, 5 min, 4°C and suspended in red blood lysis buffer (Sigma-Aldrich) and DNase (0.33U/ml, Sigma-Adrich), incubated for 5min at room temperature, washed twice with cold PBS, passed through a 40 μm mesh filter, centrifuged at 300 g, 5 min, 4°C and then resuspended in ice cold FACS buffer. Spleenocytes were either sorted fresh or INs-seq fixed and then sorted, for qPCR analysis of Actb.

Isolation of T-regulatory cells from mouse tumors and cervical lymph nodes

CD45+, TCR-β+, CD11b- and Foxp3+ (by endogenous Foxp3-RFP or anti Foxp3-APC conjugated antibody) cells were isolated from cervical lymph nodes or MCA-205 fiborosarcoma tumors from Foxp3-RFP 10 weeks, female mice.

Tumor growth measurements

8 weeks, female mice were inoculated intradermally (i.d.) with $5x10^5$ MCA-205 cells suspended in 100 μL PBS on their right flank. At day 19, tumors volume was measured using a caliper. Tumor volume was assessed by measuring two diameters and calculated using the formula $X^2 \times Y \times 0.52$ (where X, smaller diameter and Y, larger diameter).

Isolation of tumor infiltrating leukocytes

Tumor bearing mice were sacrificed at 10 and 19 days after tumor cell inoculation. The tumors underwent mechanical (gentleMACS™ C tube, Miltenyi Biotec Inc., San Diego, CA) and enzymatic digestion (0.1mg/ml DNase type I (Roche), and 1mg/ml Collagenase IV (Worthington) in RPMI-1640) for 15 min at 37°C. Cells then filtered through 100μm cell strainer, washed with ice cold sorting buffer, centrifuged (5 min, 4°C, 300 g), and stained with fluorophores conjugated antibodies.

Flow cytometry single cell sorting for Mars-seq 2.0

Following staining, cells were washed and resuspended in cold washing buffer (0.5% BSA and 2 mM EDTA in PBS), stained with fluorophore conjugated anti-mouse CD45 antibody, and filtered through a 70-μm strainer. Before sorting, cells were stained with propidium iodide to exclude dead/dying cells. Cell sorting was performed using a BD FACSAria Fusion flow cytometer (BD Biosciences), gating for CD45+ cells after exclusion of dead cells and doublets. Single cells were sorted into 384-well capture plates containing 2 mL of lysis solution and barcoded poly(T) reverse-transcription (RT) primers for scRNA-seq as described previously (Keren-Shaul et al., 2019). Immediately after sorting, plates were spun down to ensure cell immersion into the lysis solution, snap-frozen on dry ice and stored at -80°C until further processing. Cells were analyzed using BD FACSDIVA software (BD Bioscience) and FlowJo software (FlowJo, LLC).

Mass Cytometry (CyTOF)

Mouse tumor samples were processed as previously described to achieve single cell suspension. Tumor infiltrating immune cell were enriched using CD45 microbeads (Miltenyi Biotech). Cells were washed with CyTOF PBS and stained with Cisplatin viability stain for 1 min, washed twice and stained with extracellular antibodies cocktail (resource table) at RT for 30 min. After extracellular staining, cells were washed twice and fixed using the CyTOF Nuclear Antigen Staining Buffer working solution [dilute the 4X Nuclear Antigen Staining Buffer Concentrate (1 part) with Nuclear Antigen Staining Buffer Diluent (3 parts)] for 30 minutes while pipetting every 10 min. Fixed cells were permed by using the CyTOF Perm-S buffer and stained with Intracellular antibodies cocktail for 30 min. Fixed cells were washed twice and resuspended in 4% Formaldehyde (Thermo Fisher) and kept at 4°C over night until acquisition day. Stained and Fixed cells were analyzed using the CyTOF 3 (Helios) system (FLUIDIGM). Data was processed using Cytobank.

Flow cytometry bulk cell sorting for qPCR experiments

Cell populations were sorted using BD FACSAria Fusion flow cytometer (BD Biosciences). Prior to sorting, all samples were filtered through a 70-μm nylon mesh. Samples were CD11b+Gpnmb+/Pdpn+/Lyc6+ or CD11c+ MHCII high/mid or CD45+CD11b+Arg1+ or CD45+. 5,000-10,000 cells were sorted into a low-bind Eppendorf tube containing 40 μL of lysis/binding buffer (Invitrogen). Immediately after sorting, tubes were spun down to ensure cell immersion into the lysis solution, snap frozen on dry ice, and stored at –80°C until processed.

Droplet-based scRNA-seq (10x Chromium)

Fresh or INs-seq-fixed cells were FACS sorted into 0.04% PBS-BSA buffer or INs-seq collection buffer respectively. Cells were stained with trypan blue and counted using light microscopy and then loaded onto a 10x Chromium microfluidics system according to the manufacturer's guidelines. scRNA-seq 5′ gene expression (GEX) libraries were generated using the 10X Genomics Chromium Single Cell 5′ Kit v2 and the 10x Chromium Controller (10x Genomics) according to the 10x Single Cell 5′ v2 protocol guidelines. The 5′ mRNA library was sequenced with Illumina's NextSeq 500 using 75 paired-end reads.

MARS-seq 2.0 library preparation

Single-cell libraries were prepared as previously described (Keren-Shaul et al., 2019). In brief, mRNA from cells sorted into cell capture plates were barcoded and converted into cDNA and pooled using and automated pipeline. The pooled sample is then linearly amplified by T7 *in vitro* transcription, and the resulting RNA is fragmented and converted into sequencing-ready library by tagging the samples with pool barcodes and illumina sequences during ligation, RT, and PCR. Each pool of cells was tested for library quality and concentration is assessed as described. Overall, barcoding was done on three levels: cell barcodes allow attribution of each sequence read to its cell of origin, thus enabling pooling; unique molecular identifiers (UMIs) allow tagging each original molecule in order to avoid amplification bias; and plate barcodes allow elimination of the batch effect.

Suppression assay

Spleen was isolated from 11 weeks WT female (C57BL/6) mouse and was dissociated into single-cell suspension and filtered through 70μm cell strainer. Red blood cells were lysed with RBC lysis buffer (Sigma). Splenocytes were passed over CD8 T cell enrichment LS column (Miltenyi). Enriched CD8 T cells were labeled with Cell Proliferation dye eFluor™ 450 (Invitrogen) according to manufacturer's guidelines and co cultured with sterilely sorted intratumoral (MCA205) Cd11b+ Gpnmb+ or Cd11b+ Cxc3r1+ or Cd11b+ Ccr2+ cells separately in a 1:1 ratio. T cells were then activated with CD3/CD28 Dynabeads (Thermo Fisher) according to the kit guidelines. The cells were co-cultured in TC 96 well plate round bottom (Conring) in C10 medium containing recombinant IL-2 (5 ng/ml) and 100 U/mL penicillin/streptomycin. For control, T cells were solo-cultured with or without activation. Cells were harvested after 48 hours, cell suspension was stained with CD8-APC/Cy7 to gate only T cells and T cell proliferation was measured in FACS analysis by Cell Proliferation dye eFluor™ 450 dilution. For N9 murine microglia line experiment, activated CD8 T cells were co cultured with either WT N9, Trem2 knockout N9 cells (5:1), or 50ng/ml TGFb, and were incubated for 48h in 37C, 5% CO_2 incubator. Cells were analyzed for proliferation using LSRII FACS analyzer (BD).

Trem2 guide RNA cloning

For single guide RNA (sgRNA) targeting Trem2 expression, we used the lentiviral lentiGuide-mCherry backbone vector (Jaitin et al., 2016). LentiGuide-mCherry vector was digested with the restriction enzyme FastDigest Esp3I (Thermo Fisher Scientific, FD0454) and guide RNAs (See Table S7) were inserted by Gibson assembly reaction.

Lentivirus production

Trem2-guide RNA lentiviral particles were produced by transfecting 293T cells together with packaging plasmids, using the jetPEI transfection reagent (Polyplus-transfection) according to the manufacturer's instructions and following the standard lentivirus production protocol (Klages et al., 2000). Media was replaced with RPMI medium without additives 18 hours post transfection, and media containing virus particles were collected 48 and 72 hours post transfection.

Trem2 knockout N9 cell line generation

Murine microglia N9 cells (kindly provided by Prof. Frenkel D, TAU, Israel), were stably infected with CAS9 nuclease expressing lentivirus (Addgene, 52962-LV) and selected using 10 μg/ml Blastocytidin antibiotic. Cas9 expressing N9 were further infected with a mix of 4 sgRNA targeting Trem2 expressing lentivirus, followed by single cell colony isolation. Trem2 knockout was validated by qPCR (see Table S7) and western blot.

Western blot validation for Trem2 N9 cell line knock out

Membrane lysates were prepared as previously described (Schlepckow et al., 2020). Cell supernatants were collected, centrifuged (10 min at 1400 rpm) and filtrated (0.45 μm). Lysates (50 μg) and supernatants (40 μl) were separated by standard 12% SDS–PAGE, transferred onto nitrocellulose membranes (ThermoFisher Scientific). Analysis was further performed according to standard procedure using mTrem-2 antibody (Abcam #Ab86491), appropriate HRP-conjugated secondary antibody and ECL visualization.

QUANTIFICATION AND STATISTICAL ANALYSIS

Single cell RNA data processing (10x)

The Cell Ranger Single Software Suite v.3.1.0 was used to perform sample alignment, de-multiplexing and UMI counting using the default parameters. The complete spreadsheet of the sequencing metrics is presented in the Supplemental Information (See Table S6). A total of 97,257 single cells consisting of 20 samples (5 Fresh and 15 INs-seq samples) were collected, with the number of cells recovered per samples ranging from 343 to 9507. The mean reads per cells varied from 13,480 and 353,472 with median UMI of 561 to 8092 per cell. Low-quality cells were discarded if the number of expressed genes was smaller than 300. Cells were also removed if their mitochondrial gene expression were larger than 10 percent.

Chromium (10x) data integration and clustering analysis

For processing of both fresh and INs-seq scRNA-seq data, we used Seurat R package version 3.0. First, we performed filtering of the cells removing cells with less than 300 genes expressed or fraction of mitochondrial gene expression above 10 percent of total UMIs. Next, data for paired fresh and INs-seq samples were normalized using the NormalizeData function and integrated with correction for methods effects across datasets using FindIntegrationAnchors function. We performed Louvain clustering and dimensionality reduction using UMAP algorithm. Marker genes for each cluster have been identified using FindAllMarkers function and Wilcoxon test.

MARS-seq processing

scRNA-seq libraries (pooled at equimolar concentration) were sequenced on an Illumina NextSeq 500 at a median sequencing depth of ~40,000 reads per cell. Sequences were mapped to the mouse (mm10). Demultiplexing and filtering was performed as previously described (Jaitin et al., 2014), with the following adaptations: Mapping of reads was performed using HISAT (version 0.1.6); reads with multiple mapping positions were excluded. Reads were associated with genes if they were mapped to an exon, using the ensembl gene annotation database (embl release 90). Exons of different genes that shared a genomic position on the same strand were considered as a single gene with a concatenated gene symbol. The level of spurious unique molecular identifiers (UMIs) in the data were estimated by using statistics on empty MARS-seq wells, and excluded rare cases with estimated noise > 5% (median estimated noise over all experiments was 2%).

Metacell analysis

We used the R package "MetaCell" (Baran et al., 2019) to analyze data from Figures 4 and 5. We removed specific mitochondrial genes, immunoglobulin genes, and genes linked with poorly supported transcriptional models (annotated with the prefix "Rp-"). We then filtered cells with less than 400 UMIs. Gene features were selected using the parameter Tvm = 0.3 and a minimum total UMI count > 50. We subsequently performed hierarchical clustering of the correlation matrix between those genes (filtering genes with low coverage and computing correlation using a down-sampled UMI matrix) and selected the gene clusters that contained anchor genes. We used K = 100, 750 bootstrap iterations and otherwise standard parameters. Metacells were annotated by applying a straightforward analysis of known cell type marker genes (e.g., *Ear2, Cx3cr1*, *Arg1*, *Trem2*, *Cd3d, Cd79b*, and more). Subsets of Monocytes and Macrophages in Figure 5were obtained by hierarchical clustering of the confusion matrix and supervised analysis of enriched genes in homogeneous groups of metacells.

In Tables S4 and S5, we refer to the log2 of a metacell's footprint, which is the gene-wise average UMI count per metacell normalized by the median UMI count across all metacells (Baran et al., 2019).

Statistical analysis

Figure 1C. qPCR Ct values of mouse Actb cDNA after reverse transcription (cDNA-Ct) and reverse transcription followed by PCR amplification (amplified cDNA-Ct) for INs-seq BMDC and other fixation protocols. n = 4 and represents biological repeats of 5000 cells for each condition. Bars indicate mean. Error bars indicate mean ± SEM.

Figure 2G. qPCR analysis (ΔΔCt) of Tnf, Cxcl2 and Il-1b fold change in LPS-stimulated CD11c+MHCII^{high} and CD11c+MHCII^{mid} BMDC compared to control untreated BMDC. n = 3 and represents biological repeats of 5000 cells for each condition. Bars indicate mean. Error bars indicate mean ± SEM

Figures 4D and 4E. qPCR analysis (ΔΔCt) of Arg1 and Trem2 fold change in the different cell populations compared to Ly6C+. n = 4 and represents biological repeats of 5000 cells for each condition. Bars indicate mean. Error bars indicate mean ± SEM.

Figure 5F. MCA205 tumor volume of WT and Trem2 KO mice. n = 7 for WT, n = 4 for Trem2 KO. n represents number of animals, red line represents mean tumor volume. Error bars indicate mean ± SEM. One-way ANOVA statistical test.

Figure 5G. Percentage of key cell populations in WT and Trem2 KO in the MCA205 tumor microenvironment. n = 7 for WT, n = 4 for Trem2 KO. n represents number of animals. Black line indicates average percentage. Stars marking significant p value between fraction of cells in WT and Trem2 KO .One-way ANOVA statistical test.

Figure S1B. qPCR Ct values of mouse and human Actb cDNA after reverse transcription (cDNA-Ct) for INs-seq and other fixation protocols processed mouse spleen CD45+ cells and human PBMC CD45+ cells. n = 4 and represents biological repeats of 5000 cells for each condition. Bars indicate mean. Error bars indicate mean ± SEM.

Figure S1C. qPCR Ct values of mouse Actb cDNA after reverse transcription (cDNA-Ct) and reverse transcription followed by PCR library amplification (amplified cDNA-Ct) for INs-seq and fresh BMDC. n = 4 and represents biological repeats of 5000 cells for each condition. Bars indicate mean. Error bars indicate mean ± SEM.

Figure S7D. Bar plot showing the percentage of CD8 T cells proliferation (number of divisions) in the different activation and co-culturing conditions as indicated in the plot. TGF-beta treatment was added as a standard control for CD8 T cell suppression. n = 8 and represents biological repeats of 30,000 cells for each condition. Bars indicate the percentage of CD8 T cells proliferation for each number of cell divisions. Error bars indicate mean ± SEM.

Figure S7E. The percentage of T cells that proliferated calculated as area under the proliferation curve, normalized to activation condition. n = 8 and represents biological repeats of 30,000 cells for each condition. Bars indicate the percentage of T cells that proliferated, calculated as area under the proliferation curve, normalized to activation condition. Error bars indicate mean ± SEM t test.

Figure S7G. The percentage of T cells that proliferated calculated as area under the proliferation curve, normalized to activation condition. n = 8 and represents biological repeats of 30,000 cells for each condition. Bars indicate the percentage of T cells that proliferated, calculated as area under the proliferation curve, normalized to activation condition. Error bars indicate mean ± SEM t test.

Supplemental Figures

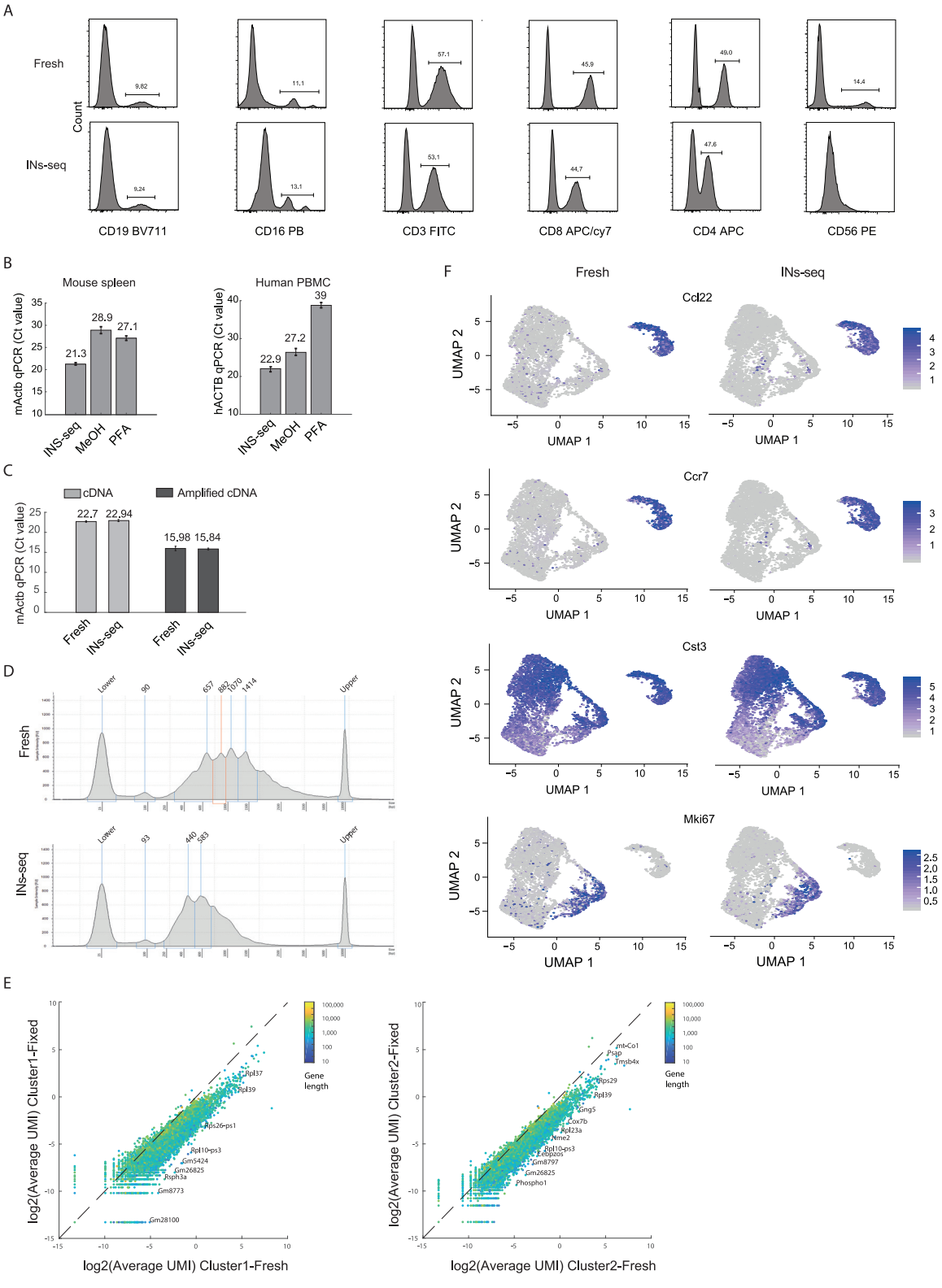

(legend on next page)

Figure S1. INs-Seq: An Integrated Technology for scRNA-Seq and Intracellular Protein Measurements, Related to Figure 1

(A) Representative FACS histogram plots of fresh PBMC (upper panel) and INs-seq processed PBMC (lower panel) stained with CD19, CD16, CD3, CD8, CD4 and CD56 antibodies conjugated to different fluorophores. (B) qPCR Ct values of mouse and human *Actb* cDNA after reverse transcription (cDNA-Ct) for INs-seq and other fixation protocols processed 5000 mouse spleen CD45+ cells (left) and human PBMC CD45+ cells (right). Error bars indicate mean ± SEM. (C) qPCR Ct values of mouse *Actb* cDNA after reverse transcription (cDNA-Ct) and reverse transcription followed by PCR library amplification (amplified cDNA-Ct) for INs-seq and fresh BMDC. Error bars indicate mean ± SEM. (D) Electrophoresis histograms of amplified cDNA processed with 10X Genomics Chromium Single Cell 5′ Kit v2 protocol from fresh BMDC (upper panel) and INs-seq BMDC (lower panel). (E) Scatterplots showing the average UMI counts (log2 scale) of INs-seq processed BMDC (y axis) compared with fresh BMDC (x axis) from cluster 1 (left) and cluster 2 (right). Colors indicate gene length. (F) Projection of differential genes on the UMAP manifold of the fresh and INs-seq BMDC data. Scale bar indicates gene expression level.

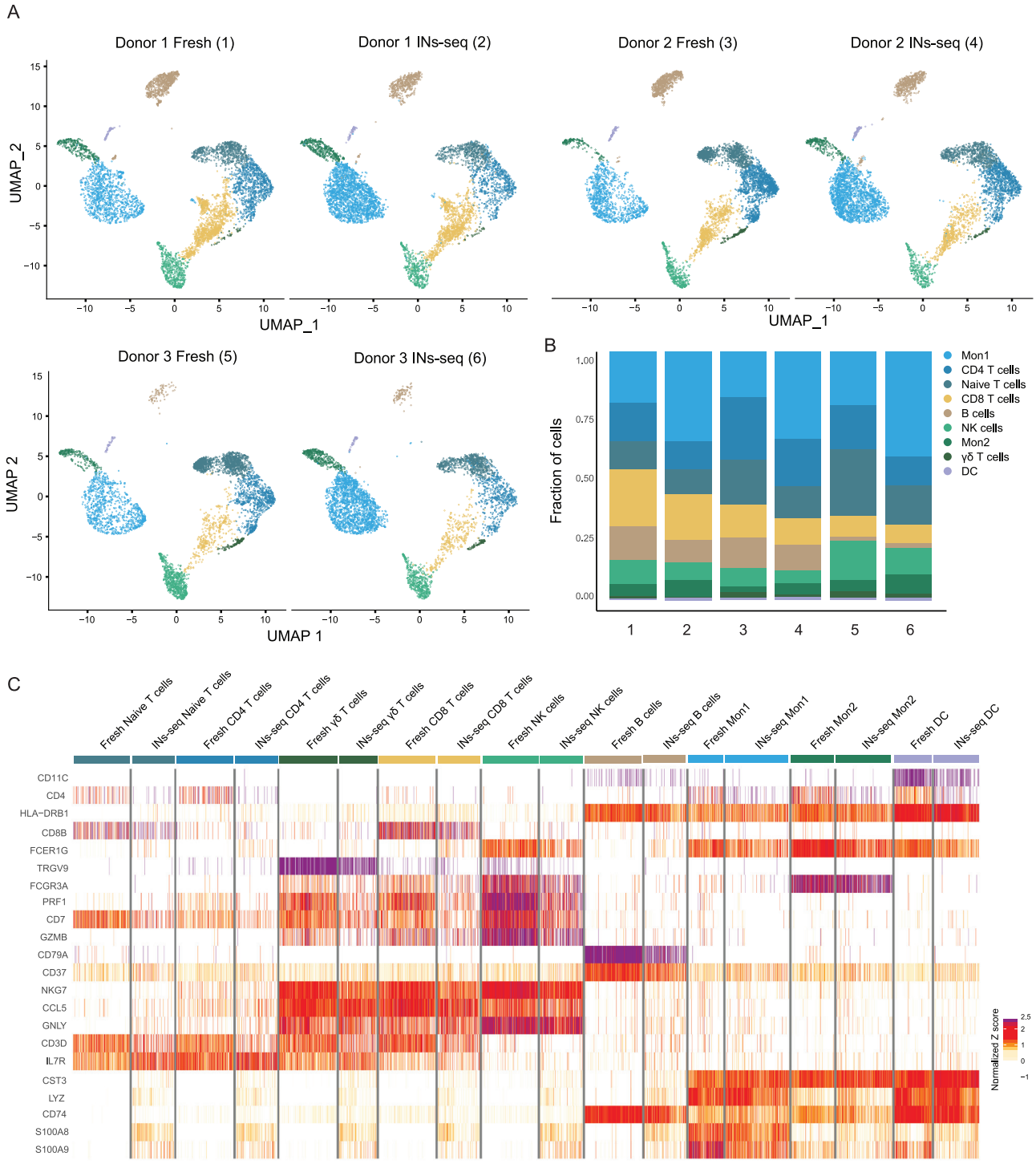

Figure S2. INs-Seq Data from Human PBMCs, Related to Figure 1

(A) UMAP of scRNA-seq data from fresh (1) 9053, (3) 4522, and (5) 5571 and INs-seq (2) 5620, (4) 4569, and (6) 9376 human blood PBMC (CD45+ immune cells) from three different healthy donors. Color code is for cell type assignment as indicated in the plot, with (B) the fraction of the different cell types in each sample. (C) Heatmap of single cells from donor 1 fresh and INs-seq CD45+ PBMC. Gene expression is compared between fresh and INs-seq samples in each cluster.

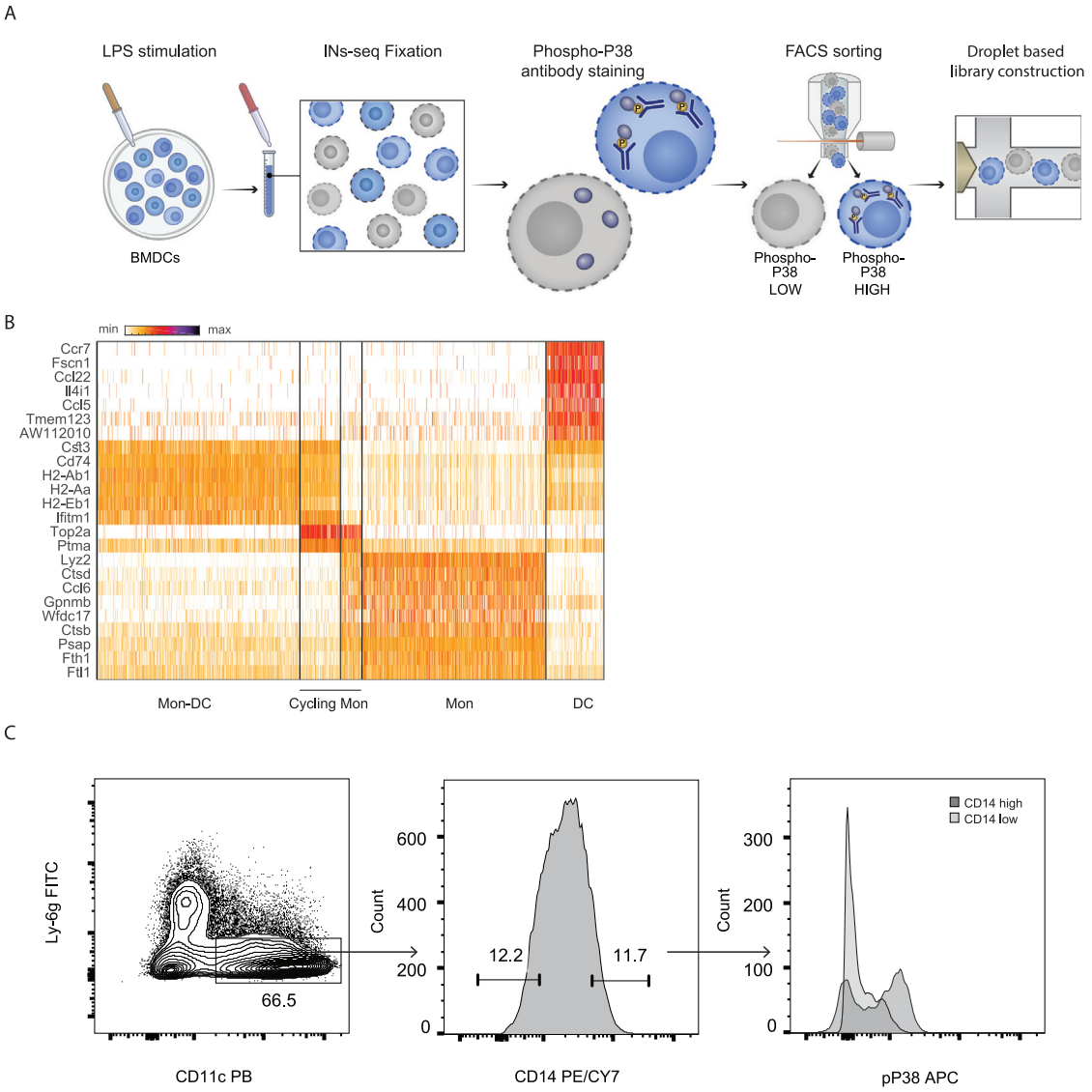

Figure S3. INs-Seq Identifies DCs as a pp38^{-} Fraction in BMDC Culture, Related to Figure 2

(A) Schematics of the experiment design. (B) Heatmap of 9623 BMDC. Gene expression of the most 24 differential genes across the clusters is shown. (C) Representative of FACS plots showing pp38 fluorescent signal among LPS stimulated BMDC populations CD11c+ CD14^{high} and CD11c+ CD14^{low}.

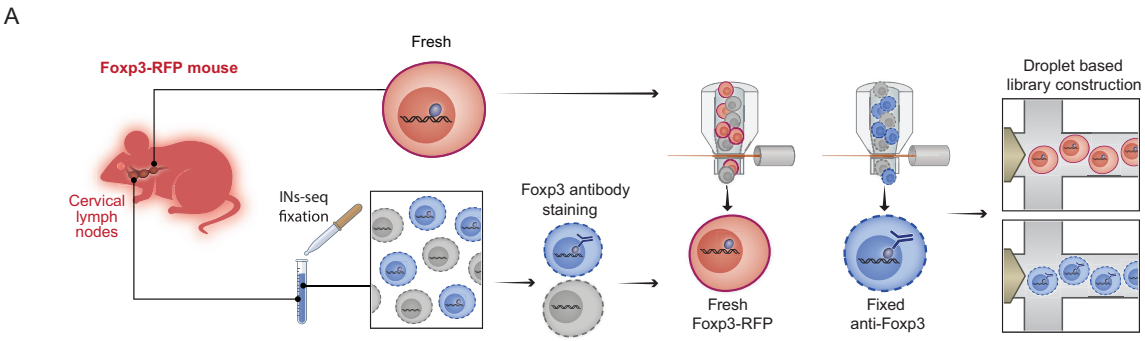

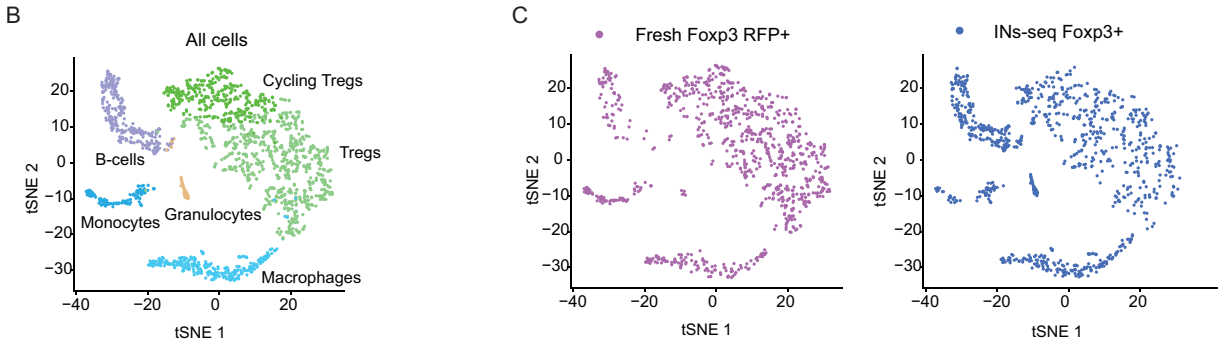

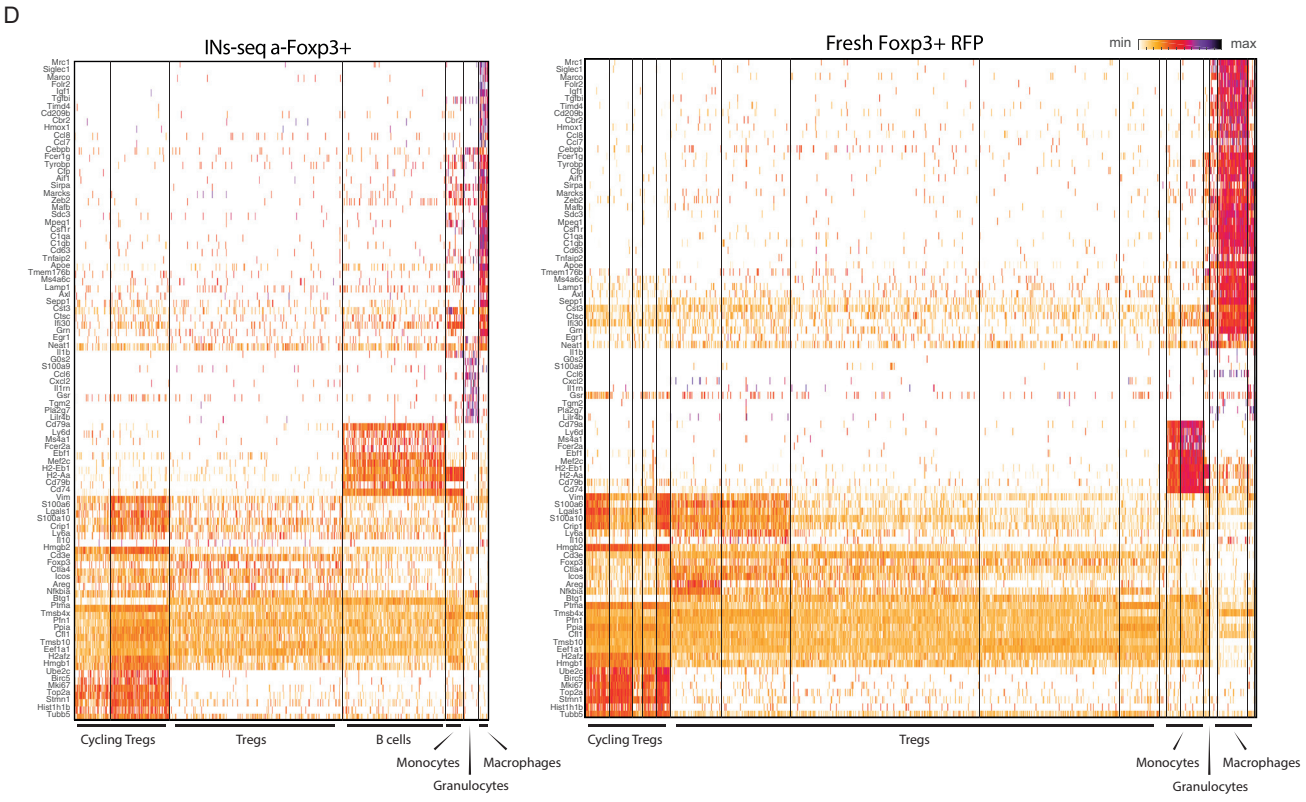

(legend on next page)

Figure S4. *In Vivo* Characterization of Foxp3$^+$ Treg Cells, Related to Figure 3

(A) Schematics of the experiment design. (B) tSNE representation of 939 fresh Foxp3-RFP$^+$ (down sampled from 4544 cells) and 939 INs-seq a-Foxp3+ cells. Color code for clustering analysis as indicated in the plot. (C) tSNE representation of fresh Foxp3-RFP$^+$ and INs-seq APC-Foxp3+ cells. (D) Heatmap of 939 INs-seq a-Foxp3+ single cells (left) and 4544 Fresh Foxp3-RFP$^+$ single cells (right). Gene expression of most deferential genes across the clusters is shown. Color code indicates gene expression.

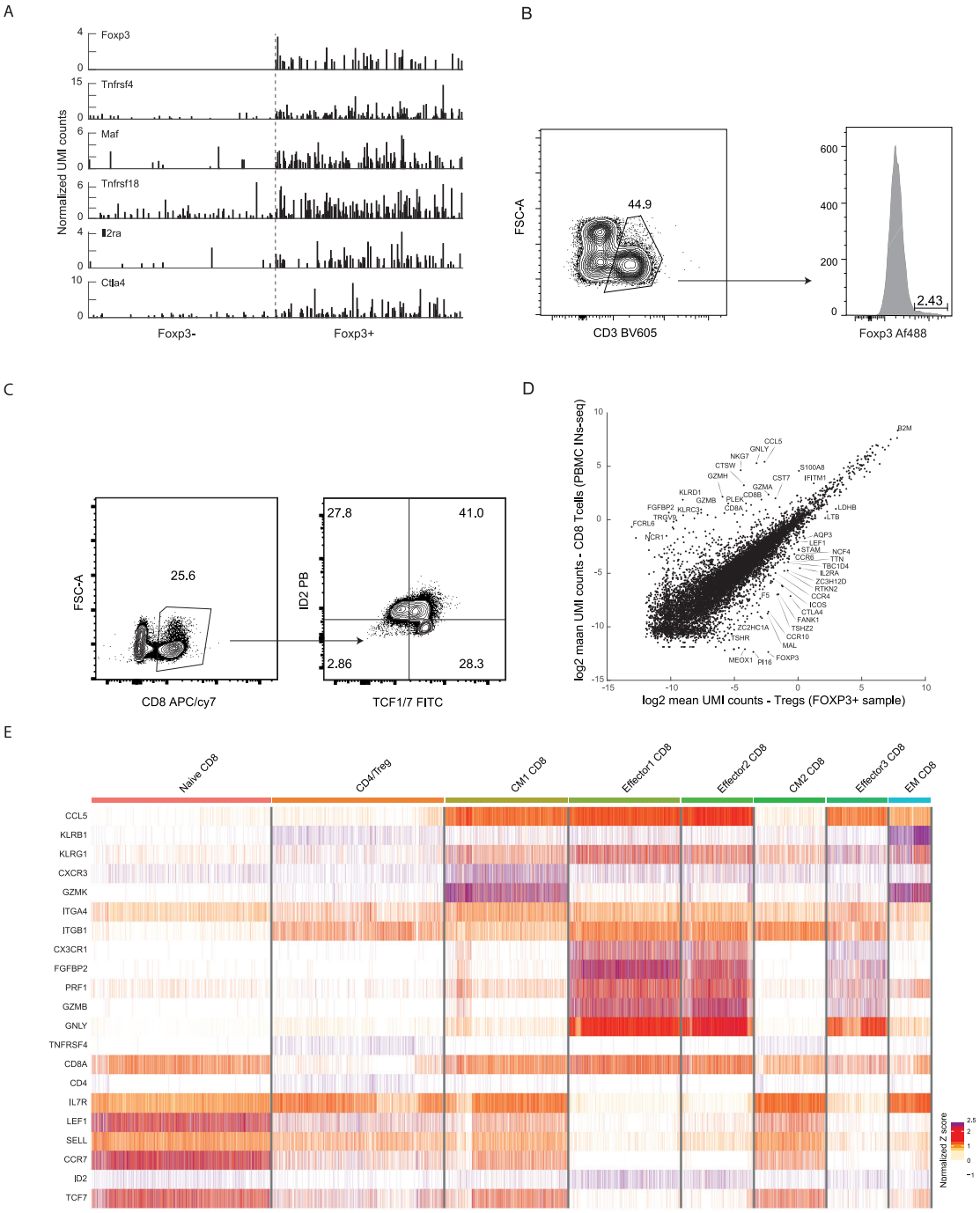

Figure S5. INs-Seq TF Map of Human T Cells, Related to Figure 3

(A) Normalized UMI count of regulatory T cells related genes in TCRb+FOXP3- (left panel) and TCRb+FOXP3+ (right panel) cells isolated from MCA205 mouse tumor. Each line represents one cell. (B) FACS plots showing gating and sorting strategy of CD3+FOXP3+ donor #2 PBMC. (C) FACS plots showing gating and sorting strategy of CD8+TCF7+ID2+, CD8+TCF7+ID2- and CD8+ TCF7- ID2+ from donor #2 PBMC. (D) Scatterplot showing the mean UMI counts (log2 scale) of CD8 T cells of donor PMBC (y axis) compared with CD3+FOXP3+ cells of the same donor (x axis). (E) Heatmap of 21 genes from 18,740 T cells clustered into 8 clusters. Color code indicates gene expression in Z score.

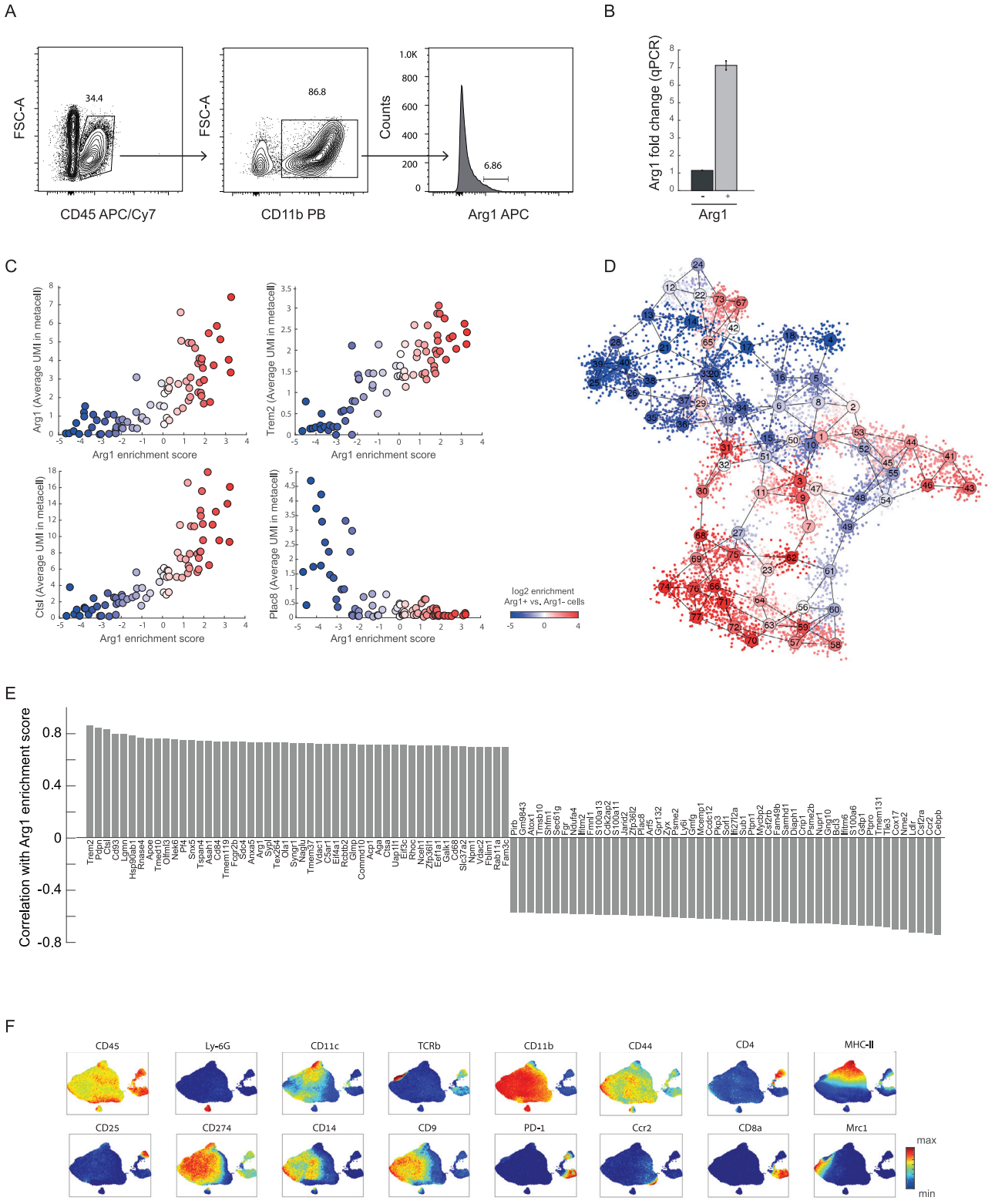

Figure S6. Trem2 Defines Two Populations of Tumor-Infiltrating Suppressive Myeloid Cells, Related to Figure 4

(A) Representative FACS plot showing sorting strategy for CD45+ CD11b+ Arg1+ cells. (B) qPCR values for *Arg1* mRNA in INs-seq Arg1+ and Arg1- cells in the TME. Error bars indicate mean ± SEM. (C) Scatterplot showing the average UMI counts for selected genes (*Arg1, Trem2, Ctsl*, and *Plac8*) in 77 metacells (y axis)

(legend continued on next page)

compared with enrichment score (log2 scale) in Arg1+ versus Arg1- cells (x axis). Scale bar indicates enrichment score. (D) Two-dimensional graph projection of 77 metacells representing 8156 Arg1+ and Arg1- cells. Color indicates log2 enrichment in Arg1+ (E) Bar plot showing the indicated genes expression (x axis) with correlation to Arg1 protein ratio (F) UMAP projection of CyTOF data of MCA205 CD45+ immune cells. Detected protein levels of the indicated proteins shown by color gradient as indicated in the plot.

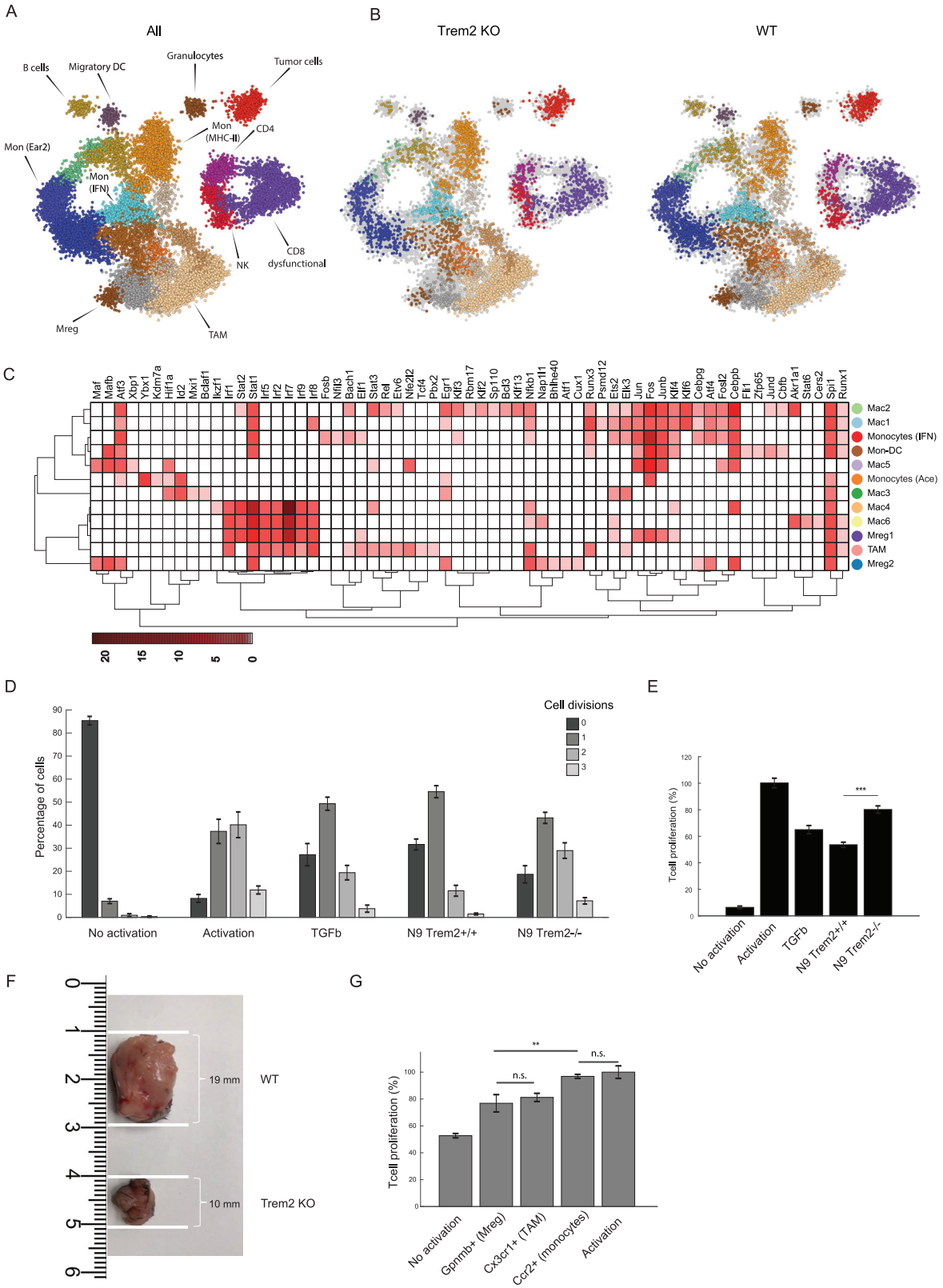

(legend on next page)

Figure S7. Trem2 Promotes T Cell Dysfunction and Tumor Immune Escape, Related to Figure 5

(A) Two-dimensional graph projection of 82 metacells representing 15,946 intratumoral CD45+ cells from MCA205 (day 19) from WT and Trem2 KO mice. (B) Highlight of cells originating from WT mice and (C) Trem2 KO mice. (C) Heatmap showing enrichment of transcription factors binding sites in the regulatory regions of 12 metacell marker genes. Only TFs with significant Normalized Enrichment Score (NES > 3.5) and average expression above 0.1 UMI in metacell are shown. (D) Bar plot showing the percentage of CD8 T cells proliferation (number of divisions) in the different activation and co-culturing conditions as indicated in the plot. TGF-beta treatment was added as a standard control for CD8 T cell suppression. Error bars indicate mean ± SEM. (E) The percentage of T cells that proliferated calculated as area under the proliferation curve, normalized to activation condition. Error bars indicate mean ± SEM (***$p < 0.001$, t test). (F) MCA205 tumor images from WT (upper tumor image) and Trem2 KO (lower tumor image). (G) The percentage of T cells that proliferated calculated as area under the proliferation curve, normalized to activation condition. Different activation and co-culturing conditions as indicated in the plot. Error bars indicate mean ± SEM (**$p < 0.01$, t test).